# Collective acceleration of ions on injection of high-current electron beams into a low-pressure neutral gas

K. Alexander and W. Hintze

*Central Institute of Electron Physics, Academy of Sciences of the German Democratic Republic, Berlin*
Fiz. Elem. Chastits At. Yadra **13**, 344–426 (March–April 1982)

A review of the experimental data on collective ion acceleration by an intense electron beam propagating in a low-pressure neutral gas is given. The model of acceleration on the ionization front developed by the authors is discussed in detail. A qualitative comparison of theoretical predictions with the experimental data is carried out.

PACS numbers: 29.15.Dt

## INTRODUCTION

In 1956 V. I. Veksler proposed the principle of collective, or, as he called it, coherent, acceleration of charged particles.[1,2] Since that time many attempts have been made to create on the basis of this general principle an accelerator which could compete with ordinary accelerators (see, for example, Refs. 3–5). The most highly developed idea of this type is the well known method of acceleration by electron rings proposed by V. I. Veksler and subsequently developed primarily by V. P. Sarantsev and his group at Dubna. According to this idea, the deep electrostatic potential well which exists inside a ring-shaped current of relativistic electrons is used for capture of ions, which are then accelerated in motion of the electron ring along its rotation axis under the influence of external forces. This method is attractive in that the external fields required for acceleration of the light electrons have a considerably lower field strength than the field of the electron ring itself, which accelerates the heavy ions.

Linear relativistic electron beams are easier to produce than electron rings. Many theoretical ideas on the creation in such beams of internal accelerating fields of sufficient strength[3] were advanced prior to the experimental observation of collective acceleration of ions in 1969. Graybill and Uglum[6] found that high-current relativistic electron beams drifting in a gas-filled tube actually accelerate ions to energies several times that of the electron beam. Other groups soon confirmed this result and obtained new experimental data. As time went on, more information, sometimes contradictory, was accumulated and attempts were made (also sometimes mutually contradictory) to explain the acceleration process theoretically. Eventually an attractive suggestion appeared for construction of a real high-energy accelerator—the idea of ionization front acceleration (IFA)[7-9]—which, however, still awaits experimental demonstration.[1)]

In such a situation it is very important to have a completely acceptable explanation or a model of the acceleration process from which one could obtain, for example, scaling laws or other relations which present interest for possible practical applications. In the present review we shall attempt to give a systematic picture of the phenomenon, based on the model of a moving ionization front. In order to demonstrate the applicability of this model and to make clear its deficiencies, it is necessary first of all to analyze systematically the existing experimental data. We shall show that certain apparently contradictory results of various experiments actually agree for an appropriate choice of the important physical parameters. We shall then attempt to show convincingly that the model proposed by us is suitable for obtaining correct scaling laws and a qualitative, and sometimes even quantitative, explanation of most of the experimental facts.

As we have already mentioned, we shall restrict the discussion to the acceleration of ions in intense relativistic electron beams passing through a gas-filled tube. Usually such beams are obtained by using a vacuum diode which consists of a cold field-emission cathode and an anode foil which is transparent for the fast electrons and which separates the diode from the gas-filled drift space (Fig. 2). In order to avoid overlap of the diode gap with the plasma and discharge, the duration of the high-voltage pulse applied to the diode, and consequently also the duration of the beam, is limited to a value of the order of $10^{-7}$ sec.[2)] The principal parameters of installations used in experiments on ion acceleration are given in Tables I–IV and in Fig. 1.

## 1. EXPERIMENTAL RESULTS

### Typical experimental apparatus and methods of diagnostics

A typical experimental apparatus for study of ion acceleration in intense relativistic electron beams is shown in Fig. 2.

A high-voltage pulse (0.2–5 MeV, 20–150 nsec) is fed to the cathode ( ), from which an electron beam is extracted as the result of field emission.[3)] A typical

[1)] "Ionization front acceleration" is the customary translation of the Russian "uskorenie na fronte ionizatsii."

[2)] We shall not consider the acceleration of ions inside the diode itself, which was first observed by A. A. Plyuto[10,11] and which has recently produced considerable interest, or experiments on acceleration in electron beams of microsecond duration, which can be obtained with use of an isolated anode and very low gas pressures.[12,13] It appears to us that the acceleration mechanisms which act in these cases differ from those of interest here and therefore deserve separate discussion.

[3)] A detailed description of the technique of obtaining relativistic electron beams can be found, for example, in the review by V. P. Smirnov.[14]

 0090-4759/82/020143-36$04.40  

TABLE I. Electron-beam parameters.

| Entry number | $E$, MeV | $I$, kA | $t_b(t_r)$, nsec | $a$, cm | References |
|---|---|---|---|---|---|
| 1 | 0,2 | 200 | 80 (—) | 1.59 | [44] |
| 2 | 0.45 | 10—20 | 70 (—) | 1.40 | [25] |
| 3 | 0,4—0.5 | 10 | 30 (8—10) | 2.5 | [26, 27] |
| 4 | 0.48; 0.89 | 60—110 | 55 (8) | 1.27; 2.54 | [33] |
| 5 | 0,5 | 160 | 50 (—) | 3.8? | [17] |
| 6 | 0.6—0.9 | 52—125 | 20 (—) | 2,54? | [32] |
| 7 | 0.65 | 15—20 | 50 (30) | 2.12 | [20, 31, 47] |
| 8 | 0.7—1.1 | 20—48 | — | 3.0 | [40] |
| 9 | 0.75 | 100 | 100 (10) | 2.54 | [22] |
| 10 | 1.0 | 25 | 50 (10; 30) | 2.12? | [43] |
| 11 | 1.0 | 25 | 50 (30) | 2,12? | [45] |
| 12 | 1.0 | 110 | 50 (—) | 3.8? | [17] |
| 13 | 1.0 | 115 | 100 (10) | 2.54 | [19] |
| 14 | 1.0 | 160 | 80 (—) | 1.59 | [44] |
| 15 | 1.3 | 35 | 50 (10) | 1,25 | [69] |
| 16 | 1.3 | 50 | 50 (35) | 2.0—2.5* | [49] |
| 17 | 1.5 | 20 | 20 (—) | — | [18] |
| 18 | 1.5—2.0 | 50—100 | 90 (70) | 0.15—1.6 | [23] |
| 19 | 1.7 | 30 | 50 (10) | 1.25 | [29, 30] |
| 20 | 2.0 | 15—20 | 50 (5) | 0.15; 0.64; 1.25 | [24, 36] |
| 21 | 2.0 | 100 | 100 (70) | 0.95 | [51, 52] |
| 22 | 2.4—5.6 | 38—88 | 160—230 (20—25) | 0.65—5.1 | [34] |
| 23 | 4,5 | 40 | 65 (—) | — | [18] |

*Tubular beam: inner and outer radii.

TABLE II. Drift-space parameters.

| Entry number | $R$, cm | $L$, cm | Gas | $p$, Torr | $B$, kG | References |
|---|---|---|---|---|---|---|
| 1 | 1.59 | 40.0 | $H_2$, He, air | 0.2; 0.01—0.065 | 0 | [44] |
| 2 | 7.5 | 200 | $H_2$, $D_2$ | — | 4.5—5 | [25] |
| 3 | 4.5 | 54—57 | air | 0.07—0.9 | 0.05—5.0 | [26, 27] |
| 4 | 3.8 | 82 | $H_2$ | 0.55 | 0 | [33] |
| 5 | 3.8 | 58 | $H_2$ | 0.034—0.96 | 0 | [17] |
| 6 | 3.8 | 82 | $H_2$ | 0.3—0.7 | 0 | [32] |
| 7 | 5.0 | 10—100 | $H_2$, $D_2$ | 0.04—0.6 | 0 | [20, 31, 47] |
| 8 | 3.5; 4.5 | 4—70 | $H_2$, He, $N_2$ | 0.015—0.04 | 0 | [40] |
| 9 | 3.8 | 82 | $H_2$ | 0.15—0.7 | 0 | [22] |
| 10 | 5.0 | 100 | $H_2$ | 0.05—0.6 | 0 | [43] |
| 11 | 5; 10 | 13—50; 40 | $H_2$ | 0.05—0.6 | 0 | [45] |
| 12 | 3.8 | 58 | $H_2$ | 0.034—0.96 | 0 | [17] |
| 13 | 3.81 | 73 | $H_2$, $N_2$ | 0.1—0.8; 0.02—0,15 | 0.1—10 | [19] |
| 14 | 1.59 | 40 | $H_2$, $N_2$, air | 0.01—0.2 | 0 | [44] |
| 15 | 7.6 | 50 | $H_2$, $D_2$, He, $N_2$ | 0.025—0.4 | 0 | [69] |
| 16 | 10 | 100 | $H_2$, $D_2$, He | 0.075—0.6 | 0—3.0 | [49] |
| 17 | 15.9 | 20 | air | 0.005, 0.01, 0.015 | 0 | [18] |
| 18 | 2.5 | 70 | $H_2$, $D_2$ | 0.15 | 0 | [23] |
| 19 | 5.0 | 50 | $H_2$, $D_2$, He, $N_2$, Ar | 0.025—0.4 | 0 | [29, 30] |
| 20 | 2.5, 5.0, 12.7 | 63 | $H_2$, $D_2$ | 0.05—0.6 | 0 | [24, 36] |
| 21 | 2.5 | 100 | $H_2$ | 0.065 | 0 | [51, 52] |
| 22 | 32 | 117 | $H_2$, $D_2$ | 0.02—0.3 | 0 | [34] |
| 23 | — | — | air | 0.08—0.16 | 0 | [18] |

value of the anode–cathode gap is of the order of 1 cm, so that a field of strength more than 1 MV/cm is produced in the diode. The total current flowing through the diode is measured by means of a return current shunt (*13*). On passing through the anode foil (usually aluminized Mylar of thickness 5–15 $\mu$m), the beam enters a drift chamber—a cylindrical conducting tube at the anode potential and filled with a low-pressure neutral gas (0.01–25 Torr).

In some cases the drift chamber is made of transparent material (glass or Plexiglas), which permits the beam to be photographed. In this case a conducting grid is placed inside the tube in order to allow flow of the return currents. The total current flowing in the drift space is measured by Rogowski belts (*12*) placed at various distances along the axis of beam travel. In some cases a magnetic guide field (0.1–10 kG) is produced in a drift space by means of coils (*2*). Inside the drift chamber one can place various targets (*3,11*) of carbon, boron nitride, or other materials suitable for nuclear activation analysis of the ions. After passing through a diaphragm of diameter 1 cm or less at the end of the drift chamber, the electron beam is deflected by a magnet (*10*), so that only the accelerated ions can enter the region in which the ion diagnostic devices are located. The magnetic field of the deflecting magnet usually has a strength in the range 0.5–1 kG. In the drift region, as the result of additional pumping, a vacuum of the order $10^{-5}$ Torr is usually produced. Methods of ion diagnostics include time-of-flight measurements based on comparison of the shape of the current signals from the screens (*9*) (as a rule these are metallic screens with an absorption coefficient of about 50%), measurement of the total ion current with a Faraday cup (*5*), nuclear activation analysis, and also

TABLE III. Ion-beam parameters.

| Entry number | Type of ions | $E_i$, MeV | $N_i$, $10^{12}$ | $\tau_i$, nsec | $I_i$, A | $l$, cm | $F$, MV/cm | $p_{opt}$, Torr | References |
|---|---|---|---|---|---|---|---|---|---|
| 1 | H | 0.84 | 10—1000 | 5—8 | — | — | — | 0.2 | [44] |
| 2 | H | 1.0 | 200 | — | — | — | — | — | [25] |
| 3 | — | — | — | — | — | — | — | — | [26, 27] |
| 4 | H | 2—12 | — | — | — | — | — | — | [33] |
| 5 | H | 0.95 | 10 | 3—5 | 530—320 | 3—7 | 0.3—0.6 | — | [17] |
| 6 | H | 5—12 | — | — | — | $\leqslant 20$ | — | 0.4—0.6 | [32] |
| 7 | H, D | 8—10; 4 | 0.8; 1,0 | 5—15 | 26: 8 | 20 | 0,1 | 0,12 | [20, 31, 47] |
| 8 | H, He, N | —; 9; — | —; —; 0.06 | 10 | 1; 1; 2 | —; —; 30 | —; —; 0.3 | —; —; 0.02 | [40] |
| 9 | H | 3—7, 5 | 1 | 3 | $\approx 50$ | — | $\geqslant 0.3$ | | [22] |
| 10 | H | 1—4; 1—3 | — | — | — | — | — | 0.45; 0.2 | [43] |
| 11 | H | 1—4 | — | — | — | — | — | — | [45] |
| 12 | H | 1.75 | 10 | 3—5 | 530—320 | 3—7 | 0.3—0.6 | — | [17] |
| 13 | H, $N^{+7}$ | 12: 29 | 0.5—2; — | 5: — | 1.5; — | 11 | 0.3 | 0.6; 0.04—0,08 | [19] |
| 14 | H | 1,4—1.8 | 10—100 | 5—8 | — | — | — | 0.2 | [44] |
| 15 | H, D, He, N | 4.8; 4,7; 8.9; 20.0 | 20; 20; 10; 6 | 3; 5; 10; 10 | 100; 80; 20; 10 | $\leqslant 20$ | $> 0.07$ | 0,05—0,3; 0,05—0,3; 0,1—0,4; 0.025—0.05 | [69] |
| 16 | H | $< 4.5$ | 10 | 5 ($B < 0.8$), 20 ($B > 0.8$) | 70 | — | — | 0.3 | [49] |
| 17 | H | — | $< 10^5$ | — | — | — | — | — | [18] |
| 18 | H | 1—5 | 0.1—100 | — | — | $\leqslant 6$ | $\leqslant 1.0$ | — | [23] |
| 19 | H, D, He, N, Ar | 5—7; 4—7; 8—9; 17—24; 8—14 | 4; 2.5; 2; 1.4 0,25 | 3; 4; 15; 15; $> 20$ | 200; 100; 20; 15; 1—2 | $\leqslant 30$ | $> 0.06$ | $\sim 0.2$; 0,03 | [29, 30] |
| 20 | H, D | $< 4.5$ | — | — | — | 25 | 0.1—0.2 | 0,1—0.25 | [24, 36] |
| 21 | H | 3 | — | — | — | 10—20 | 0,15—0,3 | 0.065 | [51, 52] |
| 22 | H, D | 14.4; 18—20 | —; 400 | — | — | — | — | —; 0.08 | [34] |
| 23 | — | — | — | — | — | — | — | — | [18] |

TABLE IV. Calculated parameters.

| Entry number | $I_e$, kA | $I/I_e$ | v/γ | $J$, kA/cm$^2$ | $R/a$ | $E_i/ZE_0$ | $d_0$, cm | $\theta_0$, nsec | $2d_0/\theta_0 c$ | References |
|---|---|---|---|---|---|---|---|---|---|---|
| 1 | 2.07 | 97 | 12.2 | 25.2 | 1 | 4 | 0.17 | 0.66 | 0.017 | [44] |
| 2 | 1.48 | 6.8—13.5 | 0.37—0.74 | 1.6—3.25 | 5.36 | 2.2 | 0.79—1.12 | 1.84—2.62 | 0.039—0.029 | [25] |
| 3 | 2.53—3.42 | 3.95—2.92 | 0.4—0.344 | 0.51 | 1.8 | — | 1.85—2.12 | 4.65 | 0.027—0.030 | [26, 27] |
| 4 | 2.20; 8.8 | 27—50<br>7—12 | 2.1—3.9<br>1.4—2.5 | 11.8—21.7;<br>3.0—5.4 | 3; 1.5 | $\leqslant 13.5$ | 0.43—0.32:<br>1.21—0.9 | 0.97—0.71:<br>1.9—1.4 | 0.03: 0.042 | [33] |
| 5 | 7.45 | $\geqslant 21.5$ | 5.51 | $>3.52$ | 1? | 1.9 | $<0.81$ | $<1.77$ | 0.030 | [17] |
| 6 | 5.23—6.78 | $\leqslant 18$ | 1.2—3.9 | 2.56—6.17 | 2? | $\leqslant 13.5$ | 0.92—0,85 | 2.08—1.34 | 0.029—0.042 | [32] |
| 7 | 4,0 | 3.75—5.0 | 0.43—0.58 | 1.06—1.42 | 2.36 | 1.8—3.5 | 1.71—1.47 | 3.22—2.79 | 0.035 | [20, 31, 47] |
| 8 | 8.91—11,6 | 2.24—4.15 | 0.55—0.95 | 0.71—1.7 | 1.17; 1,5 | $\leqslant 6$ | 1.8—2.18 | 3.94—2.55 | 0.03—0,057 | [40] |
| 9 | 7.1 | 14.1 | 2.61 | 0.914 | 5.67 | 4—10 | 0.80 | 1.38 | 0.039 | [22] |
| 10 | 6.85 | 3.65 | 0.53 | 1.77 | 2.36? | 1—4; 1—3 | 1.68 | 2.50 | 0.045 | [43] |
| 11 | 6.85; 4.53 | 3.65; 5.52 | 0.53 | 1.77 | 2.36?;<br>4.72? | 1—4 | 1.68 | 2.50 | 0.045 | [45] |
| 12 | 18.6? | $\geqslant 5.93$ | 2.32 | $>2.42$ | 1? | 1.75 | 1.44 | $<2.13$ | 0.045 | [17] |
| 13 | 10.27 | 11.2 | 2.43 | 5.67 | 1.5 | 12: 4 | 0.94 | 1.38 | 0.045 | [19] |
| 14 | 18.6 | 8.6 | 3.38 | 20.2 | 1 | 1.4—1.8 | 0.50 | 0.74 | 0.045 | [44] |
| 15 | 5.61 | 6.2 | 0.61 | 7.13 | 6.1 | $\leqslant 3.7$ | 0.96 | 1.24 | 0.052 | [69] |
| 16 | 8.7 | 5.75 | 0.87 | 7.07 | 4.44 | $\leqslant 3.5$ | 0.97 | 1.25 | 0.052 | [49] |
| 17 | 31.1? | $\geqslant 0.64$? | 0.35 | 0.025? | 1? | — | 17.5 | 21.0 | 0,056 | [18] |
| 18 | 9.46 | $>5.28$ | 0.64—0.82 | $>6.2$ | 2.5—25 | $<3.3$ | 1.11—1.29 | 1.33 | 0.055—0.064 | [23] |
| 19 | 9.6 | 3.12 | 0.42 | 6.11 | 4 | 2—3 | 1.20 | 1.34 | 0.060 | [29, 30] |
| 20 | 30—40 | 0.5—2.0 | 0.18—0.24 | 248; 13.6;<br>3.56 | 2—167 | 3 | 0.20; 0.87;<br>1.71 | 0.21; 0.9:<br>1.76 | 0.063; 0,064;<br>0.065 | [24, 36] |
| 21 | 15.0 | 6.65 | 1.22 | 35.3 | 2.63 | 1.5 | 0.54 | 0.56 | 0.064 | [51, 52] |
| 22 | 10.9—21.0 | 2.1—6.8 | 0,2—0.9 | 1—32.0 | 6.3—49 | 8 | 0.93—4.0 | 3.32—0.59 | 0.07—0.11 | [34] |
| 23 | 115? | $\geqslant 0.35$? | 0.24 | — | 1? | — | — | — | — | [18] |

measurement of the yield of secondary neutrons from the target by means of a neutron counter (*4*). In some installations the diagnostic devices are supplemented by a Thomson parabolic spectrometer consisting of collimators (*8*), a region with parallel electric and magnetic fields (*7*), and nuclear emulsions (*6*) for recording the spectrum. Information on the ion energy can be obtained also by placing absorbing foils of various thickness in front of the Faraday cup and using the range–energy relation of the particles.

An improved version of activation analysis is the technique based on use of foil packets[12,15] and permitting approximate determination of the energy spectrum on the basis of the known energy dependence of the ion range and reaction cross sections. The total number of ions can be evaluated on the basis of the number of neutrons and the known yield coefficient of the targets. For example, the reaction $^{12}C(d,n)^{13}N$ for a thick target gives one neutron for $10^4$ incident deuterons in the energy range 4–5 MeV.[16] The accuracy of the method is of the order $10^9$–$10^{10}$ ions. The activation method is described in more detail in the article by Luce.[13]

It is especially important that this method can be used in the presence of an intense background of electrons and γ rays from the electron beam. This permits the target to be placed at various points inside the experimental apparatus and allows one to obtain data on the ion flux, which, while it is averaged over time, is nevertheless resolved in space and in direction.

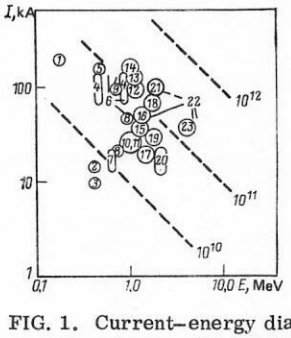


FIG. 1. Current–energy diagram of beam electrons used in experiments on collective acceleration: the dashed lines correspond to constant power values expressed in watts. The numbers indicate the entry numbers in Table I.

## Dynamics of the beam front

It was clear from the very beginning that the dynamics of propagation of the beam front is very closely related to the ion-acceleration process. We present here the results of various experiments on such questions as the dependence of the beam-front velocity on the gas pressure in the drift space, the space-time behavior of the beam front, the suppression (blocking) of the beam in vacuum, and the structure of the accelerating fields.

Experimentally the beam front is determined from the beginning of a significant rise in the total current sig-

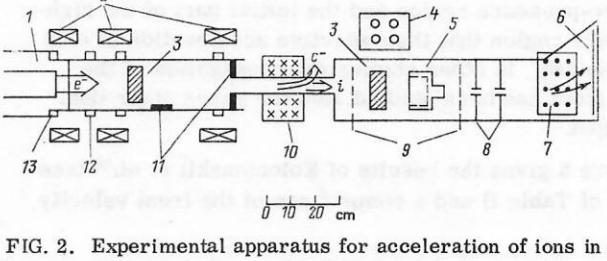


FIG. 2. Experimental apparatus for acceleration of ions in a low-pressure neutral gas: 1—diode, 2—windings which produce longitudinal magnetic field (only in certain experiments), 3—carbon blocks for nuclear-activation analysis of accelerated ions, 4—neutron counter, 5—Faraday cup, 6—nuclear emulsion for recording mass spectrum, 7—mass-spectrometer magnet, 8—spectrometer collimator, 9—screens for time-of-flight measurements, 10—deflecting magnet separating ions and electrons of the beam, 11—boron nitride or beryllium disks for activation analysis, 12—Rogowski belt for measurement of total current at various distances from the anode, 13—return current shunt.

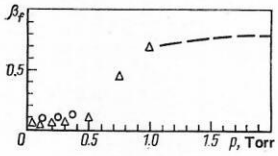


FIG. 3. Dependence of beam-front velocity $\beta_f = v_f/c$ between 12 and 54 cm from the injection point, measured by means of Rogowski belts, on the hydrogen pressure: ○—beam with energy 1 MeV (line 12 of Table I), △—0.5 MeV (line 5 of Table I), results of Rander[17,18] presented on a linear scale.

nal. This current is measured by means of Rogowski belts placed along the axis of motion of the beam. With this method of determination, the possibility of existence of a small current of fast electrons in advance of the beam front is not taken into account. The front velocity is found from the delay time of the current signal and the distance traveled.

The most striking feature observed in experiments at pressures below about 1 Torr is the very low velocity of the beam front in comparison with the velocity of the injected electrons, which amounts to more than 80% of the velocity of light at energies exceeding 0.5 MeV.

In Fig. 3 we have shown the beam-front velocity ($\beta_f = v_f/c$) between 12 and 54 cm from the point of injection as a function of the pressure of hydrogen, measured by Rander[17,18] for two different beams with energies 0.5 and 1.0 MeV, respectively (the parameters of the equipment are given in lines 5 and 12 of Table I). From the figure we can see also another interesting feature—the existence of a plateau at pressures in the region below 0.5 Torr, where the front velocity $\beta_f \lesssim 0.1$ does not depend on the pressure. Rander's results were exactly confirmed by the measurements of Ecker *et al.*,[19] as is shown in Fig. 4 (line 13 of Table I). On the basis of these measurements we shall divide the entire pressure region into a low-pressure or plateau region, a high-pressure region in which the front velocity increases with pressure, and finally the region of runaway electrons. The latter corresponds to very high front velocities comparable with the velocity of the injected electrons. We shall see subsequently that it is in the low-pressure region and the initial part of the high-pressure region that the collective acceleration of ions is observed. In other studies the propagation of the beam front has been studied also for gases other than hydrogen.

Figure 5 gives the results of Kolomenskiĭ *et al.*[20] (see line 7 of Table I) and a comparison of the front velocity

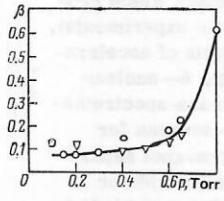


FIG. 4. Electron beam-front velocity $\beta_f$ between 6.4 and 16.5 cm from the anode, as a function of the hydrogen pressure[19] (line 13 of Table I).

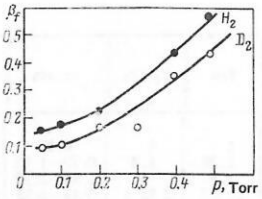


FIG. 5. Beam-front velocity $\beta_f = v_f/c$ as a function of the hydrogen and deuterium pressure.[20]

for hydrogen and deuterium. The plateau region in this case is not as clearly distinguished and extends only to pressures of 0.1 Torr. It is clearly evident that the beam-front velocity in deuterium is smaller than in hydrogen, both in the low-pressure region and in the high-pressure region.

Beam-front velocities in various gases have been studied more thoroughly by Tkach *et al.*,[21] who investigated the propagation of a beam in hydrogen, helium, nitrogen, argon, and a mixture of propane and butane. The results of these measurements, which utilized a beam with parameters 0.8 MeV, 25 kA, and 30 nsec, are given in Fig. 6. As will be shown below, the beam-front velocity is inversely proportional to the time necessary for ionization of the gas in the head part of the beam. Therefore the differences in the velocity of propagation of the beam are partly due to the difference in the ionization cross sections. These simple considerations permit explanation for the most part of the data which have been presented here.

The measurements of the beam-front velocity in hydrogen made by Drickey *et al.*[22] at various beam energies are shown in Fig. 7. It is evident that the higher energy (1 MeV—the upper curve, in comparison with 0.75 MeV—the lower curve) corresponds to a higher front velocity. In the lower curve we see the plateau region. The beam-front velocity, which we have been discussing up to this time, is determined from the time of motion of the front from the point of injection and is therefore an asymptotic value.

A very interesting feature of the beam-front motion, which is quite important also from the theoretical point of view, was observed in measurements of the beam-front position as a function of time carried out by Rander[17] and Kuswa *et al.*[23] These results are shown in Fig. 8. Various beams with energies 1.6 and 1.8

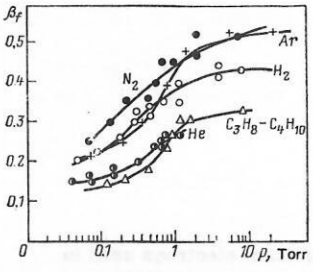


FIG. 6. Beam-front velocity as a function of pressure for various filling gases.[21] Beam parameters: 25 kA, 0.8 MeV, 30 nsec.

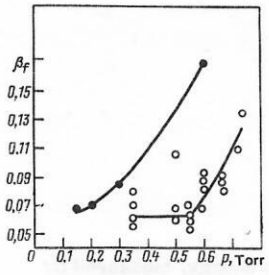


FIG. 7. Beam-front velocity measured by Drickey *et al.*[22] (line 9 of Table I). ●—Beam energy, 1 MeV, ○—0.75 MeV (the data are presented on a linear scale).

MeV and currents 43, 77, and 81 kA were injected into deuterium at a pressure 0.15 Torr. In all cases it can be seen distinctly that at the first moment there is a suppression of the beam near the anode, i.e., the beam moves very slowly for a period of the first 10–20 nsec, penetrating into the drift space only to a distance of the order of 5 cm. After this the velocity rises abruptly to its final asymptotic value. We see from this that the velocity of propagation of the beam in a low-pressure gas has a characteristic two-step structure.

It is easy to perceive, further, an explicit dependence of the beam-front velocity on the current; specifically, doubling of the current from 43 kA (curve 1) to 81 kA (curve 3) at an almost constant energy (changing from 1.8 to 1.6 MeV, respectively) leads to a decrease by a factor of two of the asymptotic velocity of the front (from $\beta_f = 0.072$ to $\beta_f = 0.031$). Exactly the same behavior is observed also for the initial velocity.

Suppression of the electron beam can also be demonstrated by measurement of the energy transferred to a calorimeter as a function of the distance to the calorimeter from the injection point. Recently Olson *et al.*[8] studied the travel of a beam in air. The results are shown in Fig. 9.

In one experiment the drift tube was filled with air at a pressure of 7 Torr. It follows from the graph that the loss in the energy carried by the beam is insignificant in a distance of 30 cm. In another experiment the drift space was separated by a distance $x = 14.6$ cm from the

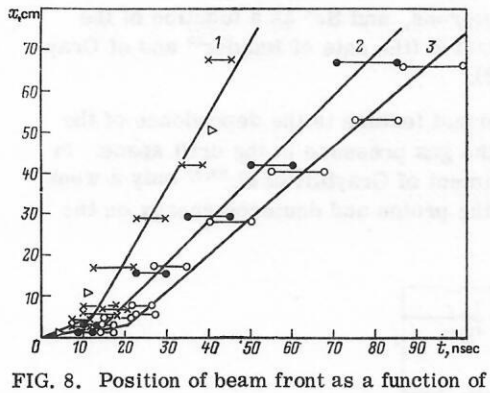


FIG. 8. Position of beam front as a function of time for various beams injected into deuterium at a pressure 0.15 Torr[23] (line 18 of Table I). Beam parameters: 1—1.8 MeV, 43 kA; 2—1.6 MeV, 77 kA; 3—1.6 MeV, 81 kA. The triangles show the results of Rander.[18]

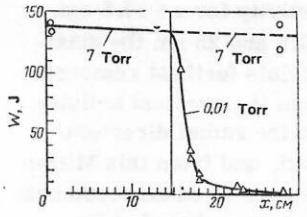


FIG. 9. Suppression (blocking) of an intense relativistic electron beam in air.[8] Calorimetric measurements of the energy transported by the beam into a drift-tube section evacuated to 0.01 Torr, as a function of the distance to the calorimeter from the aluminum foil (thickness 19 μm) at $x = 14.7$ cm separating the section with pressure optimal for beam transport from the vacuum section. Beam parameters: 0.5–0.6 MeV, 20–25 kA, 12–15 nsec; current rise time—5 nsec, beam radius $a \approx 0.5$ cm, copper drift tube radius—1.25 cm.

aluminum-foil anode of thickness 19 μm. When the region beyond the foil was evacuated to a pressure 0.01 Torr, the beam penetrated into it only to a depth of 3–5 cm (to the 10% level).

Let us consider now some experimental studies of the structure of the accelerating fields created by an electron beam in a drift space. We shall begin with indirect measurements. They are based on determination of the ion energy and the length of acceleration. We note first of all that the acceleration occurs near the anode, and the acceleration length lies roughly in the range from 5 to 30 cm. This fact has been established by many authors (as can be seen from Table I).

A more thorough study of the accelerating fields was carried out by Miller and Straw[24] (line 20 of Table I); in order to measure the flux of accelerated ions by the activation method, these authors placed small carbon targets (with a surface 2.5 × 2.5 cm) at various positions along the axis and along the radius inside the drift chamber. Since the threshold of the reaction studied, namely $^{12}C(d,n)^{13}N$, is 0.38 MeV, ions with lower energy are not detected. The results for two beams with different currents, injected into drift tubes of length 63 cm and diameters 25.4 and 12.7 cm filled with helium at 0.24 Torr, are shown in Fig. 10.

Let us discuss the cases $I/I_e = 1.3$ and $I/I_e = 2.2$ separately (we shall return later to a detailed discussion of the effect of beam current on the acceleration process).

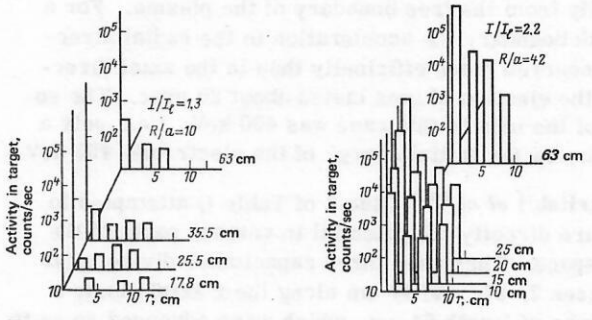


FIG. 10. Activity induced in a carbon target as a function of the radial position of the target relative to the drift-chamber axis and the distance from the anode for a deuterium pressure 0.24 Torr and for various ratios of the injected current to the limiting current[24] (line 20 of Table I).

In the first case there is no activity for $x \leq 17.5$ cm. For $x$ in the interval between 17.5 and 25 cm the maximum activity was observed at points furthest removed from the axis, while for $x > 25$ cm the greatest activity was on the axis. Ions moving in the radial direction were also independently observed, and from this Miller and Straw concluded that in this case at small distances from the anode the fields are mainly radial, but become axial in the region between 17.5 and 30 cm beyond the anode foil. For the higher current a significant activation was observed already at 10 cm from the anode, which rises rapidly with distance up to 25 cm and becomes constant for $x > 25$ cm. The maximum activity occurred on the axis, and only an insignificant number of radially accelerated ions were observed. Thus, for the higher current the acceleration occurred mainly in the axial direction. It is interesting to note that Straw and Miller found no activity in targets placed in the plane of the anode; this clearly indicates that there was no acceleration in a direction inverse to the direction of motion of the electrons of the beam. Radially accelerated ions have been observed also by other authors.

Ecker *et al.*[19] (line 13 of Table I) observed a radial flow of ions which increased with departure from the anode. They used boron nitride disks placed at distances $x = 5$, 11, and 27 cm outside openings in the chamber and recorded the reaction $^{11}B(p,n)^{11}C$, which has a proton-energy threshold 3 MeV. The drift chamber was filled with hydrogen at 0.6 Torr. At $x = 5$ cm no activity was found. Kuswa *et al.*[23] (line 18 of Table I) recorded $10^{11}$–$10^{14}$ deuterons accelerated radially to the tube walls near the anode.

A large quantity of radially accelerated ions was observed by Luce,[13] who found also that the quantities and energies of the ions accelerated radially and axially are approximately equal. It should be noted, however, that these experiments were carried out in apparatus with an isolated anode and a high vacuum, which are not the subject of our discussion. It is an interesting fact that over the entire extent of the five-meter drift tube (diameter 10 cm) ions are drawn out in radius from an electron beam with parameters 2.5 MeV, 27 kA, and duration 30 nsec. Ŝunka *et al.*[25] (line 2 of Table I) injected a beam with a previously formed plasma column and observed ions accelerated axially and radially from the free boundary of the plasma. For a smooth boundary the acceleration in the radial direction occurred more efficiently than in the axial direction; the ejection of ions lasted about 20 nsec. The energy of the ions in this case was 400 keV, i.e., only a little below the initial energy of the electrons—450 keV.

Bystritskiĭ *et al.*[26,27] (line 3 of Table I) attempted to measure directly the potential in various parts of the drift space. They used three capacitance dividers (at distances 7, 27, and 47 cm along the $x$ axis) inside a drift tube of length 54 cm, which were advanced so as to reach the edge of the electron beam. In more than a hundred measurements at $10^{-3}$ Torr and in the presence of a longitudinal magnetic field of 3.1 kG they found that the ratio of the potentials on probe 1 (near the anode)

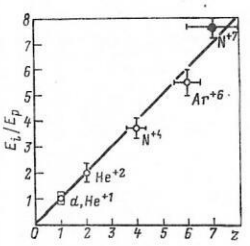


FIG. 11. Ion energy (relative to proton energy) measured by means of a spectrometer, as a function of the charge state of the ions.[18] Added data: □—Graybill[6] (deuterium); ●—Ecker.[19]

and probe 2 (in the center) was $\varphi_1/\varphi_2 = 1.2 \pm 0.3$. The absolute value of the potential on probe 2 was $140 \pm 20$ kV, which on the assumption of a uniform beam gives $280 \pm 40$ kV on the axis. Thus, the potential even on the axis at the anode (340 kV) is definitely lower than the energy of the injected electrons. This is inconsistent with the assumption of a deep potential well in the theory of Olson[28] (see Sec. 2 of the present work). We note, however, that the measurements of Bystritskiĭ *et al.* were not carried out under the usual conditions for acceleration of ions, since a strong magnetic field was present. In addition, no details were given in Refs. 26 and 27 regarding the time dependence of the potential. We are proceeding from the assumption that maximum values were given.

### Ion energy

We shall discuss here measurements of the energy of the accelerated ions and shall establish important dependences on the gas pressure, the current and energy of the beam electrons, and the charge state and mass of the ions.

The ion energy relative to that of protons accelerated under the same conditions is shown in Fig. 11 as a function of the charge state $Z$. (To Rander's results[18] we add the data on $N^{+7}$ obtained by Ecker.[19]) It follows from the figure that the ion energy is directly proportional to their charge state over a wide range $Z = 1$–7 for masses from 1 to 14 proton masses. These data show in addition that the ion energy does not depend on their mass (compare $N^{+4}$ and $N^{+7}$). This also can be seen from Fig. 12, in which we have plotted the energy of protons, deuterons, and $He^{+}$ as a function of the mass for constant $Z$ (the data of Rander[18] and of Graybill and Uglum[6]).

Another important feature is the dependence of the ion energy on the gas pressure in the drift space. In the first experiment of Graybill *et al.*[29,30] only a weak dependence of the proton and deuteron energy on the

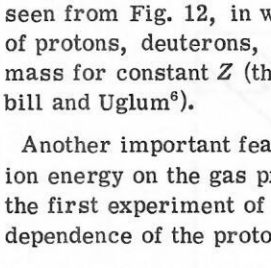


FIG. 12. Ion energy (relative to proton energy) as a function of mass for a constant charge state.[18] The data for deuterium are from Ref. 6.

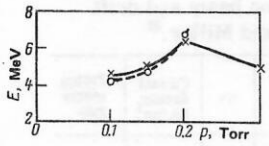


FIG. 13. Energy of protons and deuterons accelerated by an electron beam with parameters 1.7 MeV, 30 kA as a function of pressure[29,30]: ×—hydrogen, ○—deuterium.

gas pressure was observed (Fig. 13), but the situation changes at higher pressures. The results of Drickey *et al.*[22] which show a dependence of the proton energy on the hydrogen pressure, are given in Fig. 14. Both curves show a rapid increase of energy on increase of the pressure up to 0.7 Torr. The upper curve corresponds to an electron energy 1 MeV, and the lower to 0.75 MeV. The gain in energy also increases, i.e., the ratio of the ion energy to the electron energy; for the upper curve it reaches 12 times, and for the lower curve 10 times. It can be seen also that for a given pressure the ion energy increases with increase of the energy of the beam electrons.

Qualitatively the same behavior of the ion energy was observed by Kolomenskiĭ *et al.*,[20,31] as can be seen from Fig. 15. These authors found a large energy gain at a pressure 0.3 Torr—more than 15 times (an electron beam with energy 0.65 MeV accelerated protons to 10 MeV). In that work a further important feature was observed— a decrease of the ion energy at higher pressures. This can be seen more distinctly from the data of Ecker and Putnam,[32] which are shown in Fig. 16. There is a certain value of the pressure, $p_{co}$, above which the ion acceleration process is cut off. We shall return to this point later.

The dependence of the ion energy on the electron beam current was for some time the subject of disagreement. The first experiments of Graybill and Uglum[6] showed explicitly that the ion energy increases as the square of the beam current. In reality, however, these authors varied the beam current, changing the voltage for a fixed diode geometry, so that they simultaneously varied both the current and the electron energy, as a result of which these experiments must be interpreted with caution. Many authors, nevertheless, have taken the quadratic dependence of the energy on the beam current as an experimental fact. However, more careful experiments carried out by Ecker and Putnam[32,33] showed that for a fixed energy of the electron beam the ion energy falls off with increase of the current. The energy of the protons as a function of the beam current for beam energies 0.89 and 0.48 MeV is given in Fig. 17. In both cases a doubling of the current leads to a decrease of the energy by about 50%. The drift gas was hydrogen at 0.55 Torr, and the cathode radius was 2.54 cm. All experimental parameters were maintained constant except for the current, which was varied by changing the anode–cathode gap, i.e., the impedance of the diode.

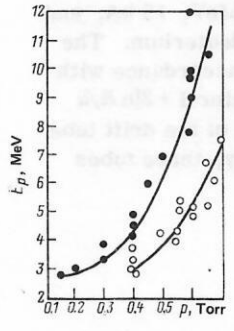


FIG. 14. Final value of proton energy as a function of hydrogen pressure. The upper curve corresponds to an electron beam energy 1 MeV,[19] and the lower curve to 0.75 MeV.[22] In both cases the cathode radius is 2.54 cm.

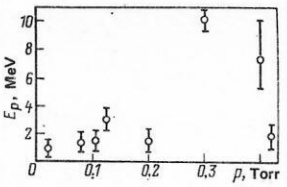


FIG. 15. Final energy of protons as a function of hydrogen pressure.[20,31] The energy of the electron beam is 0.65 MeV (line 7 of Table I).

In another series of experiments of the same authors the proton energy was measured as a function of the diode impedance. These data are shown in Fig. 18. The drift tube was as before filled with hydrogen at 0.55 Torr, but now two cathodes with different radii were used ($r_c = 1.27$ and 2.54 cm). As follows from Fig. 18, the higher proton energy corresponds to the larger cathode radius for the same impedance value. Identical impedance values do not necessarily mean equality of the currents and voltages individually. On the assumption that the beam radius is proportional to the cathode radius, these data suggest that an increase of the beam current density leads to a reduction of the ion energy.

This suggestion has actually been confirmed by detailed studies of Straw and Miller,[36] who in fact intended to discover the dependence of the acceleration characteristics, especially the ion energy, on the Budker parameter $\nu/\gamma$ (see Sec. 2).

These authors used electron beams with various parameters, as can be seen from Table V. The rise time

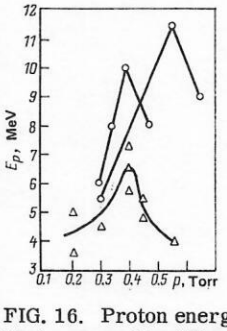


FIG. 16. Proton energy as a function of hydrogen pressure. We have combined the data of Ref. 22 (triangles) and Ref. 32, which demonstrate the pressure cutoff effect.

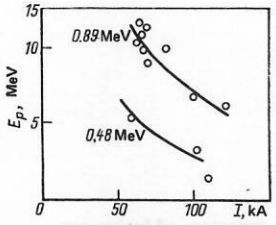


FIG. 17. Proton energy as a function of beam current for two values of electron energy. The drift gas is hydrogen at 0.55 Torr, and the cathode radius is $r_c = 2.54$ cm.[33]

of the current was 20 nsec, and the pulse duration was 100–230 nsec with variation of the impedance from its smallest value to its largest value. The drift tube had a radius $R = 32$ cm and a length $L = 117$ cm and was filled with hydrogen or deuterium at pressures in the range from 0.02 to 0.3 Torr.

As can be seen from Table II, the energy of the protons increases with increase of the peak current value. At first glance this is inconsistent with the data of Ecker and Putnam,[33] which are shown in Fig. 16. It should be noted, however, that these authors fixed all parameters including the cathode radius, whereas Straw and Miller changed the cathode diameter. The conclusion of Straw and Miller[34,35] that increase of $\nu/\gamma$ leads to an increase of the energy is erroneous. This is confirmed also by one of the results of Ecker and Putnam (see Fig. 3 of Ref. 32), according to which an increase of the parameter $\nu/\gamma$ from 1.2 to 3.9 leads to a decrease of the proton energy by more than a factor of two. The problem is resolved if one looks at the current density in the two cases. Then we finally reach the conclusion that the ion energy falls off with increase of the beam current density.

In the preceding subsection we already mentioned that the acceleration length lies in the range from 5 to 30 cm. This can be demonstrated by measurement of the energy acquired by the ions as a function of the distance traveled from the anode. Results of such measurements carried out by Kolomenskiĭ *et al.*[20] are shown in Fig. 19, in which the upper limit of the proton energy spectrum and the energy corresponding to its maximum are shown as functions of the distance. It can be seen that approximately 30 cm is required for acceleration of protons to the maximum energy. It is also obvious that the effective accelerating fields fall off with increasing distance from the anode.

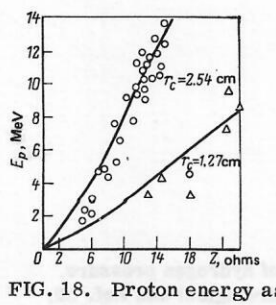


FIG. 18. Proton energy as a function of the diode impedance $Z$ at a hydrogen pressure 0.55 Torr for two cathode radii.[32,33]

TABLE V.* Parameters of the electron beam and drift chamber in the experiments of Straw and Miller.[34]

| Diode number | Cathode diameter, cm | Anode-cathode gap, cm | Peak voltage, MV | Peak current, kA | $I/I_e$ | $\nu/\gamma$ | Current density, kA/cm$^2$ | Proton energy gain |
|---|---|---|---|---|---|---|---|---|
| 1 | 1.3 | 6.7 | 5.6 | 42 | 1.9 | 0.2 | 31.6 | — |
| 2 | 1.3 | 6.4 | 5.0 | 40 | 2.0 | 0.2 | 30.1 | 3 |
| 3 | 1.3 | 6.0 | 4.7 | 38 | 2.6 | 0.2 | 28.6 | — |
| 4 | 5.1 | 15.0 | 4.9 | 45 | 2.3 | 0.3 | 2.2 | — |
| 5 | 5.1 | 5.1 | 2.9 | 56 | 5.1 | 0.5 | 2.7 | 4 |
| 6 | 5.1 | 4.8 | 2.8 | 58 | 5.6 | 0.5 | 2.8 | — |
| 7 | 10.2 | 6.2 | 3.0 | 80 | 4.8 | 0.6 | 1.0 | 6 |
| 8 | 10.2 | 5.0 | 2.4 | 88 | 7.9 | 0.9 | 1.1 | — |

*The table in this form is given in the work cited (see also line 22 of Table I), except for the last two columns. The current density was calculated on the basis of the peak current value and the radius of the beam, which is assumed equal to the radius of the cathode. The maximum gain in the ion energy (that is, the ratio of the maximum proton energy to the peak value of the voltage on the diode) was determined from Fig. 3 of Ref. 34.

### Characteristics of the ion beam

We have presented above the experimental data regarding the maximum energy to which ions are accelerated. Let us also consider in more detail the characteristics of the ion beam.

First of all let us consider the important results of Straw and Miller,[36] which show that a necessary condition for acceleration of ions is an excess of the current of the injected electron beam $I$ over the electrostatic limiting current $I_e$. Then let us turn to data on the dependence of the number of ions on the pressure and the length of the drift chamber, on the shape of the ion-current pulses, and the energy spectrum. Then we shall discuss the important questions of synchronism of the motion of the electron beam front and the ion bunch, and also the position of the ion bunch in the beam. Finally, we shall present data on measurements of the charge state of accelerated heavy ions and shall give an experimental proof of the selective acceleration of ions with the highest ratios $Z/M$ from a mixture of gases. As will be shown below (see Sec. 2), these data impose severe restrictions on possible theoretical models of ion acceleration.

Straw and Miller[36] (line 20 of Table I) investigated the influence of the ratio of the injected current to the limiting current on the ion acceleration process, using an electron beam with parameters 2 MeV, 15 kA, and 45 nsec and a drift space filled with deuterium. The limiting current value was varied in accordance with its dependence on the geometrical factor $1 + 2\ln R/a$ (see Sec. 2), by variation of the radii of the drift tube and of the electron beam. Specifically, three tubes

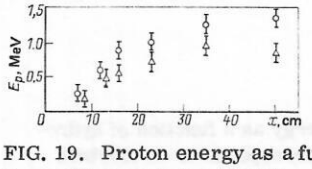


FIG. 19. Proton energy as a function of acceleration length[20]: ○—maximum proton energy, △—energy corresponding to the maximum of the spectrum.

TABLE VI. Influence of the limiting current value on ion acceleration[24,36] (line 20 of Table I).

| Ratio of radii of drift tube and electron beam,* $R/a$ | Ratio of injected current to limiting current, $I/I_e$ | Maximum energy of ion beam at target, J | Average ion energy for maximum beam energy, MeV | Pressure of deuterium at maximum energy, Torr |
|---|---|---|---|---|
| 2 | 0.54 | — | 0.5 | — |
| 4 | 0.86 | — | 0.5 | — |
| 8 | 1.2 | $2\cdot10^{-2}$ | 1 | 0.06 |
| 10 | 1.3 | $3\cdot10^{-2}$ | 1.6 | 0.1 |
| 20 | 1.6 | 0.2 | 2.3 | 0.2 |
| 84 | 2.2 | 2.9 | 3.1 | 0.25 |
| 167 | 2.8 | 1.9 | 2.8 | — |

*The electron-beam parameters are: 2 MeV, 15 kA, 45 nsec; the filling gas is deuterium.

were used, of length 63 cm each and with radii 2.5, 5.0, and 12.7 cm. The electron beam also had three different diameters (0.3, 1.27, and 2.5 cm), which were determined by the diameters of three flat cathode caps. Seven combinations were used. The ratio $R/a = 4$ was encountered twice with different $R$ and $a$, respectively, and served to check the consistency.

Detection and analysis of the accelerated deuterons was accomplished by means of carbon targets (dimensions $3.8 \times 3.8$ cm) on the basis of the existing energy threshold 0.33 MeV of the $^{12}C(d,n)^{13}N$ reaction, detection of which was carried out on the basis of secondary neutrons and by an independent activation analysis. Energy spectra were obtained also by placement of packets of aluminum foils (thickness 13 $\mu$m) in front of the carbon targets and measurement of the activity.

The results of these measurements are given in Table VI. In this table we give the pressure at which the energy deposited in the target by the ion beam was greatest, the maximum value of the beam energy, and the average energy of the ions for a given pressure (found from the spectrum) as a function of the ratio of the injected current to the limiting current. We have also included in this table the more recent data of Miller and Straw[24] for a higher ratio $I/I_e = 2.8$.

The most important conclusion from these data is that for acceleration of ions the injected current must exceed the limiting value. It is evident also that the acceleration process is very sensitive to the current near this threshold. Increase of the current to the limiting value, from 1.3 to 2.2, for example, increases the total energy of the ion beam by two orders of magnitude.

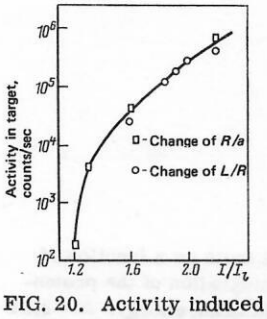


FIG. 20. Activity induced in a carbon target as a function of the ratio of the injected current to the limiting current.[41]

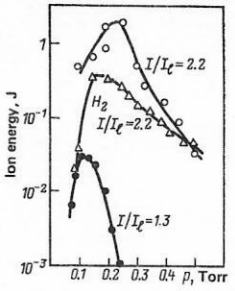


FIG. 21. Total energy of ion beam at the target as a function of the pressure of the filling gas (hydrogen and deuterium) for various ratios of the injected current to the limiting current.[24]

This effect follows from all electrostatic theories of ion acceleration, which will be discussed in detail below, and was pointed out by Alexander[37-39] and later by Olson.[28]

The threshold effect was experimentally confirmed also by Bystritskiĭ *et al.*, who varied the limiting current as the result of change of the drift-tube diameter. They found that there is no acceleration of ions until the injected current exceeds the limiting current by 1.3–1.4 times, which approximately corresponds to the data of Straw and Miller.

Study of Table I shows that in all experiments on ion acceleration the injected current has exceeded the electrostatic limit. If the length $L$ of the drift tube becomes comparable with its diameter, the limiting current increases as the result of edge effects (see Sec. 2). Therefore the ratio of the current to the limiting current can also be varied by changing the length of the tube, leaving all other parameters unchanged.

Miller and Straw observed[24,41] that the number of accelerated ions (determined from the activity in the target) rises rapidly with increase of $I/I_e$ both as the result of the change of $L/R$ and as the result of the change of $R/a$ (Fig. 20). The edge effect also explains the decrease of the energy and of the number of ions for the largest ratio $I/I_e = 2.8$ in Table III (which was calculated without taking into account this effect), since in this case the ratio $L/R$ was only equal to 1.6, whereas in all remaining cases the end plate was sufficiently far from the anode ($L/R \geq 5$). The integral charac-

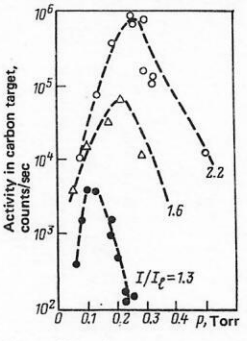


FIG. 22. Activity in a carbon target as a function of the deuterium pressure for several values of the ratio $I/I_e$.[24]

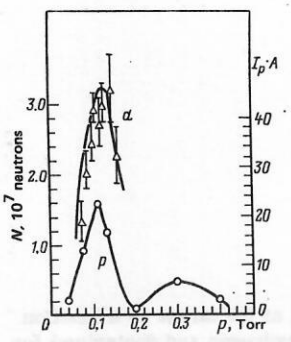


FIG. 23. Yield of neutrons from the reaction $C^{12}(d, n)N^{13}$ and proton current, as a function of drift-gas pressure.[31]

teristic of the acceleration efficiency used by Straw and Miller, namely the total energy of the ion beam at the target, depends strongly on the gas pressure. The results of the corresponding measurements of Miller and Straw[24] are shown in Fig. 21, in which data on hydrogen and deuterium have been combined. The measurements show that there is an optimum pressure value which increases with increase of the ratio of the current to the limiting current (see also the last column of Table II).

Obviously the total energy of the ions is determined by the kinetic energy and the number of ions. The total number of accelerated ions depends on the pressure in approximately the same way as the total energy. This is shown for deuterium in Fig. 22, in which the induced activity in the target is shown as a function of pressure for various ratios $I/I_e$. The similarity of the curves means that the shape of the ion spectra is insensitive to change of pressure in the experiments of Straw and Miller.

In addition, it can be seen quite clearly that increase of $I/I_e$ from 1.3 to 2.2 leads to an increase in the number of ions almost by three orders of magnitude. This, incidentally, can also be seen from Fig. 10. Similar results on the dependence of the number of ions on pressure have been obtained by many authors.

Kolomenskiĭ *et al.*[20,31,42] have investigated the acceleration in hydrogen and deuterium (Fig. 23), and Graybill[6,30] studied the acceleration of ions also in helium (Fig. 24). Bystritskiĭ *et al.*[40] found for nitrogen a very low optimal pressure (Fig. 25). In Fig. 26 we have shown the average proton current, obtained by integration of the proton current signal, as a function of the

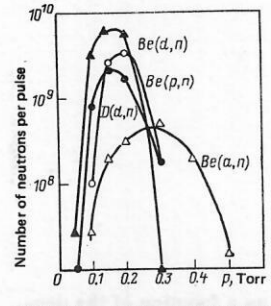


FIG. 24. Total neutron yield from the reactions $Be^9(x, n)$ and $D(d, n)$ as a function of filling-gas pressure.[6,30]

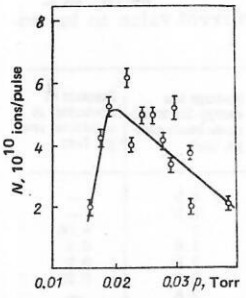


FIG. 25. Number of accelerated nitrogen ions as a function of drift-gas pressure.[40]

hydrogen pressure (the data of Drickey *et al.*[22]). In these measurements electron beams were used with two energies (0.75 and 1 MeV) and cathodes of two diameters (2.54 and 5.08 cm). Comparison of the curves for energy 1 MeV shows that the larger cathode diameter corresponds to a larger proton flux.

Summarizing, we can formulate the following general rule for the dependence of the number of ions on pressure. There are three regimes in pressure. At low pressures the number of ions is small but increases with pressure and reaches a more or less broad maximum, which represents the second regime. Finally, at still higher pressures the number of accelerated ions drops rapidly.

As will be shown in the next section, the division into regimes on the basis of pressure made here is closely related to the classification of the pressure regions made above on the basis of the beam-front velocity.

The number of accelerated ions depends on the axial position of the detector. This was already shown in Fig. 10. In Fig. 27 we have given the corresponding dependence measured by Kolomenskiĭ *et al.*[31,42] They used a cup-shaped carbon target placed at various distances from the anode inside a drift space filled with deuterium, and recorded the reaction $^{12}C(d, n)^{13}N$ by means of a neutron counter. We can note the rapid rise of the number of ions at a distance of the order of 30 cm from the anode, which indicates a characteristic length of acceleration. This agrees with the results of the same authors in study of the dependence of the ion energy on the length (see Sec. 1, Fig. 19). Beyond $x = 50$ cm a slow drop is observed, which indicates a loss of ions, the causes of which will be discussed below. If the drift tube is short ($L \leq R$), there should be a strong dependence of the number of ions on the tube length, since

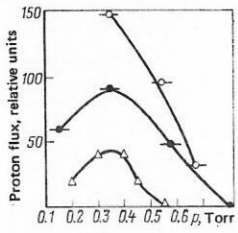


FIG. 26. Flux of protons in relative units as a function of hydrogen pressure, calculated by integration of the proton-current signal.[22] Cathode radius and beam energy: △— 2.54 cm, 1 MeV; ●—5.08 cm, 1 MeV; ○—5.08 cm, 0.75 MeV.

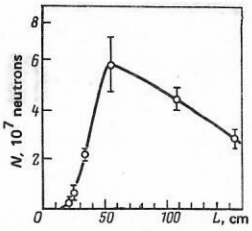


FIG. 27. Neutron yield from the reaction $C^{12}(d, n)N^{13}$ as a function of the axial location of the carbon target.[31]

for decrease of $L$ the limiting current rises and the ion-acceleration criterion ($I > I_e$) is destroyed. This dependence is already contained implicitly in Fig. 20.

The dependence of the number of ions on the drift-tube length was also determined by Bystritskiĭ *et al.*[40] The results obtained with injection of a beam with a current of 40 kA into a drift tube filled with nitrogen are shown in Fig. 28. For hydrogen and helium it was also found that the number of ions drops below the noise level for a drift-tube length less than its diameter. The decrease of the ion intensity for $L > 50$ cm, according to the explanation of these authors, is due to the decrease of the angular aperture of the spectrometer.

Up to this time we have given only the integrated characteristics of the accelerated ions, measured mainly by means of nuclear reactions, i.e., values averaged over energy and time. Let us now discuss the energy spectra and the shape of the current pulses. The accelerated ions appear mainly in the form of short pulses, typical shapes of which are shown in Fig. 29.[6,29,30] The current of accelerated ions of various gases was measured by a probe placed approximately 50 cm from the anode. The maximum proton current of 200 A with a width at half-height 5 nsec was obtained at a hydrogen pressure 0.15 Torr.

On increase of the ion mass the pulse width increases, while the maximum current value drops. We note further the rapid rise and slow fall of the current in all cases. It is also interesting to trace the ion bunch during its drift. This was done by Graybill *et al.*[6] and by Bystritskiĭ *et al.*,[40] who obtained oscillograms of the ion current in various parts of the ion diagnostics section. Graybill *et al.* found that the shape of the current pulse does not change in traveling distances of 60 cm, using three current screens at $x = 0$, $x = 30$, and $x = 60$ cm, while the maximum current value drops by about 10%. On the other hand, Bystritskiĭ *et al.* found that the width of the bunch of nitrogen ions doubles in a distances of 36 cm. The difference in the behavior of these two cases is evidently due to the difference in the

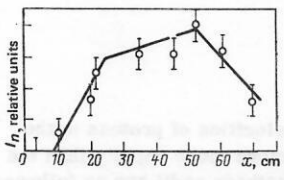


FIG. 28. Accelerated ion current as a function of drift-tube length.[40]

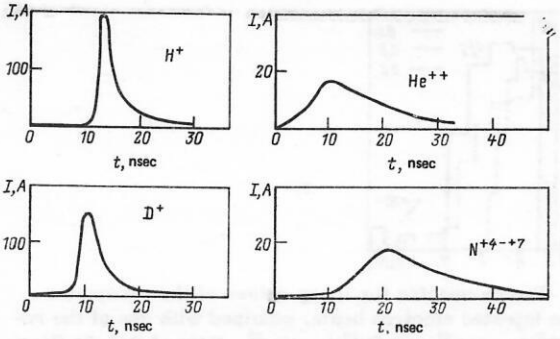


FIG. 29. Typical shapes of the ions pulses.[6,29,30] The filling-gas pressure and the delay time $t_0$ relative to the electron-beam current are as follows: hydrogen—0.15 Torr, $t_0 = 30$ nsec; deuterium—0.15 Torr, $t_0 = 40$ nsec; helium—0.2 Torr, $t_0 = 45$ nsec; nitorgen—0.025 Torr, $t_0 = 70$ nsec.

energy spectrum: a broad spectrum leads to broadening of the pulse, while for a narrow spectrum the initial shape of the current pulse is retained for a greater length.

Before going over to the energy spectrum, let us discuss the interesting case of the double pulses observed in certain experiments.[17,18,40] By double pulse we mean two separate pulses, similar in shape to those shown in Fig. 29, separated by a time interval from 5 to 60 nsec. In most cases the current in the first bunch was greater, but the reverse situation has also been observed.[18] In addition, it was found[18] that the interval between the pulses decreases linearly with increase of pressure (at 0.2 Torr it is 60 nsec, while at 0.8 Torr the pulses are completely merged).

Another type of double pulse has been observed by Ecker.[43] He studied the time dependence of the ion current and found that after the usual short pulse (single or double) there is a pause of duration more than 100 nsec and then a slow but very long rise of the ion current is observed for at least 100 nsec. Other authors, however, do not mention this effect.

The energy and momentum spectra of the accelerated ions have been determined by a number of authors, who used spectrometers or the foil-packet technique.[18,20,24,34,42,44] Typical spectra of protons and deuterons obtained by means of foils are shown in Fig. 30 (Ref. 24) and Fig. 31 (Ref. 34), in which the ion energy is plotted relative to the kinetic energy of the injected elec-

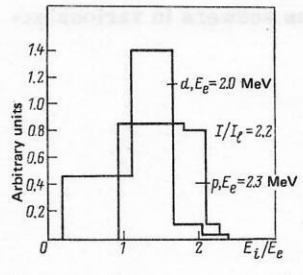


FIG. 30. Energy spectra of protons and deuterons at a filling-gas pressure 0.24 Torr and $I/I_e = 2.2$ (Ref. 24) (line 20 of Table I). The ion energies have been normalized to the kinetic energy of the electrons, absolute values of which are indicated in the figure.

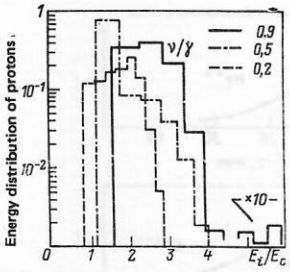


FIG. 31. Proton spectra for three values of the parameter $\nu/\gamma$ of the injected electron beam, obtained with use of the reactions $Ti^{47}(p,n)Va^{47}$ and $Cu^{63}(p,n)Zn^{63}$. Data of Ref. 34 (line 22 of Table I). The parameters of the electron beams used are given in Table II.

trons. We can see from Fig. 30 that both the proton and deuteron spectra are broad, the average ion energy being about $1.5E_e$ and the maximum energy only about $2E_e$. The proton spectra in Fig. 31, which were obtained with various geometries and beam parameters, are shown as a function of $\nu/\gamma$. Details can be found in Table II. In regard to quantitative relations, the gain in energy here is higher (up to six times). A qualitatively new feature of the spectrum for the highest $\nu/\gamma$ value is of more interest. In this case a distinct separation of the spectrum is observed into a high-energy part which contains only a small fraction of the ions, and a low-energy part which contains the main fraction of the ions. The same structure is found in the momentum spectra observed by Rander.[17,18] A typical example is given in Fig. 32, which shows the momentum spectrum of protons accelerated by a beam with energy 1 MeV in air. The spectrometric results of Kolomenskiĭ *et al.*[20] for hydrogen and deuterium at $p = 0.12$ Torr are shown in Fig. 33. In these spectra there is no double structure. It is interesting, however, that in less than 1% of all accelerator tests with a 0.5-MeV beam Kolomenskiĭ *et al.*[45] also obtained a double structure of the spectrum. One group of ions had an energy of about 1.2 MeV (the high-energy part), and the remaining ions were concentrated near 1.0 MeV.

Let us now consider the problem of synchronization of the motion of the beam front and the ion bunch. In this connection we need to discuss here two different questions: first, are the velocities correlated and, second, is there a correlation between the position of the beam front and that of the ion bunch? These two questions have received various answers in various ex-

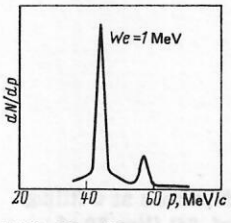


FIG. 32. Momentum spectrum of protons, obtained on injection of an electron beam with energy 1 MeV into air. The first peak corresponds to a proton energy 1.03 MeV, and the second to 1.73 MeV.[18]

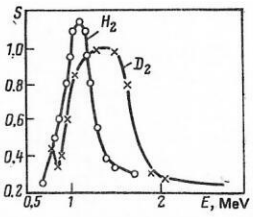


FIG. 33. Energy spectrum of accelerated protons and deuterons at a filling-gas pressure $p = 0.12$ Torr and a drift-chamber length $L = 50$ cm (Ref. 20) (line 7 of Table I).

perimental studies. We shall first give the results relating to the velocities. A correlation diagram for the proton and beam-front velocities obtained by Drickey *et al.*[22] is given in Fig. 34. It is easily seen that in almost all cases the accelerated protons have a higher velocity than the electron beam front. Variation of the velocities was achieved by changing the electron beam energy (0.75–1.0 MeV) and the cathode radius (1.27–2.54 cm).

Rander[17] found that the average proton velocity (averaged over the pressure region from 0.03 to 0.25 Torr) is approximately equal to the beam-front velocity (Table VII).

Finally, Graybill[29] reached the conclusion that the beam front is propagated significantly more rapidly than the accelerated protons. A similar conclusion can be drawn from the data of Kolomenskiĭ *et al.*[20] Calculating the ion velocities from the spectra in Fig. 33, we find for protons $\beta_p = 0.043–0.055$ and for deuterons $\beta_d = 0.03–0.044$. These values must be compared with the beam-front velocities $\beta_f = 0.18$ and 0.1 for protons and deuterons, respectively (see Fig. 5). A more detailed discussion of these questions will be given below.

In regard to the relative location of the ion bunch and the beam front, Drickey *et al.*[22] state that the proton trajectories extrapolated from time-of-flight measurements using screens in the ion-diagnostics section always lie either in the head part of the beam or directly behind it.

Graybill[29,30] found that the ions are not in the front of the beam but clearly behind it. Finally, the data of Ecker *et al.*[19] given in Fig. 35 show that the accelerated ions (protons and nitrogen ions) are far behind the front (up to 50 cm). This was observed in almost all cases

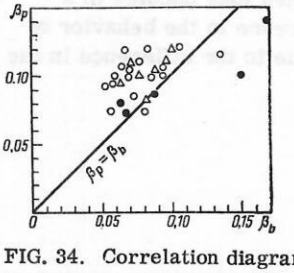


FIG. 34. Correlation diagram of velocities of protons in the beam front, showing that the ions move more rapidly than the front.[22] The beam energy and the cathode radii are as follows: △—0.75 MeV, $r_c = 1.27$ cm; ●—1.0 MeV, $r_c = 2.54$ cm; ○—0.75 MeV, $r_c = 2.54$ cm.

TABLE VII. Comparison of electron beam-front velocity in hydrogen with the proton velocity averaged over the pressure interval from 0.03 to 0.25 Torr.[17]

| Electron beam energy, MeV | Beam-front velocity* $\beta_f = v_f/c$ | Average velocity of protons* $\beta_p = v_p/c$ |
|---|---|---|
| 0.5 | 0.046±0.005 | 0.045±0.004 |
| 1.0 | 0.061±0.007 | 0.061±0.002 |

*Statistical errors are given (± one standard deviation).

both in hydrogen (0.15–0.65 Torr) and in nitrogen (0.035–0.095 Torr). The contradictions in the data on the relative location of the ion bunch in the beam will be removed in the next section by a careful analysis of the distinctions between the beam front, determined from the rapid rise of the signal by means of the Rogowski belt, and the head part of the beam, which takes part in ion acceleration.

In concluding this subsection we turn to the interesting fact that the electron beam accelerates preferentially particles with the highest charge-to-mass ratios. This effect of selective acceleration has been observed incidentally in many experiments. The significance of this effect, which is important from the theoretical point of view, was first pointed out by Alexander *et al.*,[46] and the subsequent measurements of Kolomenskiĭ *et al.*[47] qualitatively confirmed the theoretical predictions.

Here we shall give first the results of the spectrometric analysis of the charge states of accelerated ions carried out by Graybill.[29,30] He observed that on injection of a beam into helium at a pressure 0.2 Torr only $He^{++}$ is present in the accelerated ion bunch, and not $He^{+}$. However, for nitrogen at 0.25 Torr $N^{+7}$ ions have the maximum intensity, while charge states $N^{+3}$ and lower are lost. Graybill concludes that the particles with the highest $Z/M$ values are preferentially accelerated.

Rander[17] reports that in each pulse the beam accelerates both protons and partially ionized gas atoms and makes the suggestion that the acceleration of protons in cases when $H_2$ was not the filling gas is probably due to contamination of the vacuum system and to outgassing.

A detailed analysis of the selective acceleration process was made by Kolomenskiĭ *et al.*,[47] who used various concentrations of hydrogen and deuterium as filling gas and detected ions by means of a spectrometer. Their results are given in Table VIII. It can be seen that, as was mentioned previously, even with filling by pure deuterium more than 50% of the accelerated ions are protons, the appearance of which (according to the statement of the authors) is due to contamination of the

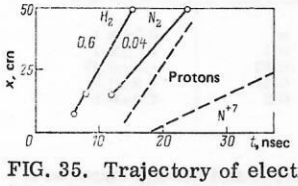


FIG. 35. Trajectory of electron beam front and ion bunches (hydrogen at 0.6 Torr; nitrogen at 0.04 Torr).[19]

TABLE VIII. Acceleration of ions from a mixture of hydrogen and deuterium.[47]

| Concentration of gases, % | | Energy of ions, MeV | | Intensity of ion beam, relative units | |
|---|---|---|---|---|---|
| $H_2$ | $D_2$ | $E_p$ | $E_d$ | $S_p$ | $S_d$ |
| 100 | 0 | 1.1±0.1 | — | 0.3—1.0 | — |
| 90 | 10 | 0.8±0.1 | — | 0.5 | — |
| 50 | 50 | 0.8±0.1 | 0.7±0.1 | 0.05—0.3 | 0.03 |
| 10 | 90 | 0.7±0.1 | 1.0±0.1 | 0.04 | 0.05—0.1 |
| 0 | 100 | 0.7±0.1 | 1.1±0.1 | 0.05 | 0.1—0.3 |

vacuum system. These data clearly indicate the high selectivity of the acceleration process to the light components.

## Other dependences

Having set forth above the main part of the experimental material, let us turn now to several experiments on the change of additional external parameters. We shall discuss the influence of a longitudinal magnetic guide field, the influence of spatially rising or falling pressure (pressure gradient), and effects occurring on change of the duration of the electron beam front. Application of a longitudinal magnetic field greatly affects the acceleration process. In order to have an idea of the characteristic magnitudes, we shall estimate first the order of magnitude of the self-field of a typical electron beam.

If a beam of radius 2 cm carries a current of 40 kA, then the azimuthal magnetic field at the edge of the beam is 4 kG. This was the strength of the self-field of the beam used in the experiments of Ecker *et al.*[19] The external field was varied from 0.1 to 10 kG. They found that a field of 0.1 kG does not affect the acceleration process, while fields of 0.2, 0.5, 3, and 10 kG led to disappearance of the accelerated protons at all momenta except one. This is the well known fact of the suppression of ion acceleration by a longitudinal magnetic field, which has been noted by many authors (see, for example, Ref. 48). Ecker *et al.*[19] report further that in an exceptional pulse (one of two at 0.5 kG) they observed protons with the same energy as without a magnetic field (3 MeV), but their flux was two to three orders of magnitude smaller.

Different results were obtained by Robertson *et al.*[49] (Table I, line 16), who used a special arrangement and observed a positive effect from introduction of a magnetic field. They injected a hollow beam (with inner diameter 4 cm and outer diameter 5 cm) into a cusp[4)] with its center 10 cm beyond the anode and with a width of 9 cm at a radius 2.5 cm. In addition, they applied a longitudinal magnetic field constant over a length of 1 m, the strength of which could be varied up to 3.2 kG. In Fig. 36 we have shown the number of accelerated ions as a function of the magnetic field strength. Hydrogen and deuterium at a pressure 0.3 Torr were used as

[4)]A region of change of direction of the magnetic field, used for conversion of the longitudinal momentum of electrons into rotational momentum, and vice versa.

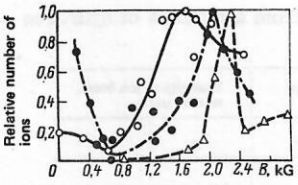


FIG. 36. Relative number of ions as a function of the magnetic field strength[49] (line 16 of Table I). The number of ions was determined from the neutron yield from the reactions indicated and from the total charge in a Faraday cup and normalized to the maximum value: △ and dashed curve are the Faraday-cup data; ○ and solid line are from $^{12}C(d, n)$; ● and dot–dash line are from $^{7}LI(p, n)$.

filling gas. For both gases the signals from the Faraday cup and the neutron yield from nuclear reactions show that after a minimum at 0.8 kG the efficiency of ion acceleration increases up to a well expressed maximum in the vicinity of 2.0 kG and then drops rapidly on increase of the field strength to 2.6 kG. Robertson *et al.*[49] further noted the following. First, when the windings of the coil producing the cusp were connected so that their fields had the same direction, no neutrons were observed from the $^{7}Li(p, n)^{7}Be$ reaction. Second, measurements with the reaction $^{12}C(d, n)^{13}N$ showed that the maximum number of ions in the presence of a magnetic field was five times greater than in the absence of the field.

In the opinion of Robertson *et al.*,[49] the decrease of the number of ions at 0.8 kG is due to the usual suppression of ion acceleration by a magnetic field as reported, for example, by Ecker *et al.*,[19] while the magnetic field corresponding to the maximum coincides with the field which provides maximum transformation of the electron momentum at the cusp.

Under similar conditions Tajima *et al.*[50] obtained $10^{11}$ $\alpha$ particles accelerated to 2.2 MeV in the presence of an axial magnetic field of strength 10 kG. The beam parameters were 0.32 MeV, 12 kA, and 100 nsec. However, these authors gave no additional information.

Using the classical arrangement, Bystritskiĭ *et al.*[27] (line 3 of Table I) studied the influence of a strong magnetic field on the process of charge neutralization in injection of an electron beam into hydrogen, helium, and air, as a function of the pressure. Specifically, they measured the voltage on a capacitance divider located at a distance of 7 cm beyond the anode foil and determined the charge-neutralization time, which was assumed to be equal to the time during which the voltage reached the anode potential. Comparison of measurements at $B = 3.1$ kG and $B = 0$ in the range of pressures from 0.1 to 1.0 Torr showed that for all gases the presence of a magnetic field slows down neutralization processes by about 50%.

The influence of a pressure gradient of the gas along the drift tube has been studied in three papers. The main idea behind this work is to use the dependence of the beam-front velocity on pressure (as was shown above) to control the motion of the front. Tkach *et al.*[21] produced a pressure differential from 0.2 Torr near the anode to 1–2 Torr at the end of a 3-meter drift tube and found that the velocity of the front actually increases by 1.4–1.6 times, depending on the gas used.

Swain *et al.*[51] and Kuswa[52] studied the influence on the ion energy of a pressure rising or falling in the direction of motion of the beam, using a time-of-flight technique. They did not find an increase of the ion energy or an appreciable change of the beam-front velocity determined by streak photography for a rising pressure. For a falling pressure they recorded a decrease of the ion energy to less than 1 MeV in comparison with 5 MeV for a constant hydrogen pressure of 0.1 Torr. In this case the pressure gradient was produced by admission of an amount of gas into the region near the anode of a previously evacuated drift tube. At the moment of injection of the beam the pressure front propagated to a certain distance from the anode. Thus, the beam first moved in the gas and, reaching the pressure front, was injected into the vacuum. This means that in reality the acceleration of ions occurred more in the vacuum than in the low-pressure gas. Time-of-flight measurements show, in confirmation of this, that ions having a rather broad energy spectrum are captured into the acceleration regime at the pressure front. The number of ions increases by 2–10 times in comparison with constant pressure.

Kolomenskiĭ *et al.*[47] produced, instead of a smooth gradient, a pressure jump by dividing the drift chamber by a foil at a distance of 13 cm from the anode. The first section contained hydrogen at 0.12 Torr, which corresponds to the optimal conditions for uniform filling. In Table IX we have given the maximum ion energy obtained for various pressures in the second chamber. It can be seen that only for $p_2 = 0.12$ and 0.15 is there some increase of energy in comparison with the case of uniform filling. Further, since the aluminum foil of thickness 75 $\mu$m absorbs the protons accelerated in the first section, we can conclude that the ions are accelerated in the second chamber. It is interesting to note that even with equal pressures in the two sections, some positive effect due to the thin foil is observed.

As a whole these data show that use of a pressure gradient clearly does not lead to a substantial improve-

TABLE IX. Maximum energy of ions in the case of a step in pressure* (Ref. 47).

| Foil | $p_1$, Torr | $p_2$, Torr | $E_p$, MeV |
|---|---|---|---|
| None | 0.12 | | 1.7±0.1 |
| Al, 70 $\mu$m | 0.12 | 0.1 | 0.5±0.1 |
| | | 0.12 | 0.4±0.1 |
| | | 0.2 | 0.45±0.1 |
| 5 $\mu$m of Mylar | 0.12 | 0 | 0.7±0.1 |
| | | 0.1 | 1.4±0.1 |
| | | 0.12 | 1.8±0.15 |
| | | 0.15 | 1.9±0.3 |
| | | 0.2 | 1.0±0.1 |

*$p_1$ and $p_2$ are the pressures in the first and second chambers, respectively.

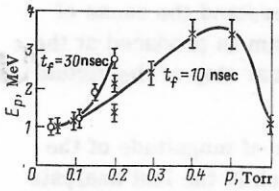


FIG. 37. Effect of beam-current rise time on the relation between ion energy and pressure.[45]

ment in the efficiency of the acceleration process. We shall return to this circumstance below.

There is an additional interesting experiment of Kolomenskiĭ *et al.*[45] in which the influence of the current-front duration on the pressure dependence of the ion energy was studied. The results of these experiments for current rise times of 10 and 30 nsec at a beam energy $E_e = 1$ MeV are given in Fig. 37.

From these data one can conclude, first, that the ion energy does not depend on the beam-current front duration and, second, that the optimal pressure shifts towards higher values if the beam-current rise time is decreased.

## 2. THEORY OF COLLECTIVE ACCELERATION OF IONS IN HIGH-CURRENT RELATIVISTIC ELECTRON BEAMS

### Introduction

Many attempts have been made to explain theoretically the existing experimental data on acceleration of ions in a low-pressure neutral gas. These theories diverge in their explanation of the origin of the accelerating fields, invoking electrostatic, induction, and wave mechanisms (see the critical discussion of these theories by Olson[53,54]).

A still greater number of new collective acceleration schemes have been proposed, using electron beams of various shapes, propagating in gas, plasma, and vacuum, in the presence of external magnetic fields and without them, with uniform and nonuniform drift-chamber velocities, and so forth.

For some time only two models have been able to compete seriously in explanation of the experimental data: the localized pinch or constriction model (LPM) of Putnam,[55-57] and the ionization-front model (IFM), which has been developed by several authors, including the authors of the present review.[28,37-39,46,58-64]

The local pinch model is based on the assumption of force-free motion of an unperturbed electron beam. For this it is required that the negative charge density of the electron beam $-en_e$ be partially compensated by a background of positive ions $en_i$ to a degree $\varkappa$ given by the relation[65]

$$\varkappa \equiv n_i/n_e = 1/\gamma^2, \qquad (1)$$

where $\gamma$ is the relativistic factor of the beam electrons [their kinetic energy is $mc^2(\gamma - 1)$].

According to the assumption, the equilibrium of the radial forces is destroyed by the localized bunch of ions. This bunch attracts to itself the beam electrons, which leads to appearance of a constriction in front of it. The compressed electron beam creates a potential well which in turn attracts the ion bunch. In the LPM synchronous motion of the ion bunch and the constriction is postulated, which would have to lead to the observed high energies of the ions.

Although this idea is extremely attractive, its initial assumption (1) of force-free motion of the beam is not satisfied in any of the experiments listed in Table I. This was first noted by Olson and Poukey,[66,67] who showed that in typical experimental situations the beams can propagate only in the case when they are almost completely charge-neutralized.

There are serious difficulties in explanation in the framework of the LPM of the principal dependences [for example, the LPM predicts a quadratic dependence of the ion energy on the electron beam current, which according to the experimental data (see Fig. 17) is erroneous]. Numerical modeling on the basis of the LPM[68] showed that for typical parameters (1 MeV, 21–96 kA) the postulated synchronous motion is maintained only for a short time and is subject to instabilities. Finally, ion energies only of the order of the electron kinetic energy were obtained, which again is inconsistent with experiment, in which a gain in energy is observed which in some cases exceeds an order of magnitude.

The same authors showed that to contain the ion bunch in the radial direction even for a certain length of time it is necessary that the beam current exceed the Alfven–Lawson limit, which we represent in the form

$$\nu/\gamma > 1 \qquad (2)$$

[here $\nu = I(\text{kA})/17\beta$ is the Budker parameter[69]; $\beta$ is the longitudinal velocity of the electrons in units of the velocity of light]. Study of Table I showed that acceleration of ions is observed also for very low values of $\nu/\gamma$. As a result we reached the conclusion that the LPM cannot be considered as the main mechanism of acceleration.

On the other hand, the ionization-front model is actually capable of explaining (qualitatively and in most cases quantitatively) the main regularities found in the experiments. We shall discuss the ionization-front model here in detail and give a comparison with the experimental data.

### Ionization-front model (IFM)

*Electrostatic suppression.* The IFM is based on the underlying fact that an intense electron beam cannot propagate in vacuum if its current exceeds a certain limit $I_e$ which we shall discuss below. The negative space charge of the beam leads to a so-called sagging of the potential (relative to the zero potential of the boundaries of the drift space, including the anode foil); if it is equal to the voltage applied to the diode, back reflection of the electrons occurs. This phenomenon is called electrostatic suppression of the beam. The region in which stopping of the electrons occurs is

called the virtual cathode. Electrostatic beam suppression can be understood on the basis of the following considerations regarding the formation of the electron beam in the diode.

We shall first consider the one-dimensional problem in which physically important changes occur only along the axis of the system (the $x$ axis). For a diode this means that we shall consider the case in which the size of the anode–cathode gap $d'$ is small in comparison with the cathode radius $r_c$. If a high voltage $U$ is applied to the diode, an electric field $E \approx U/d'$ is created which accelerates electrons from the cathode to the anode. If sufficient energy is supplied in the external circuit to maintain the voltage, and the transient processes are completed, which requires a time of the order of the inverse plasma frequency of the electron beam, then the electron flux through the diode will be limited by space charge, and the current will be determined only by the applied voltage and the diode geometry. The electric field at the cathode surface decreases to zero in this case, and electrons are emitted from the cathode with a very low (thermal) velocity which can be considered zero in comparison with the final (relativistic) velocities at the anode. The high-energy electrons pass through the foil practically without obstruction. What occurs now beyond the anode foil if the drift chamber is pumped to a high vacuum?

For the stationary state discussed here, the hydrodynamic approximation is physically adequate; this approximation is completely described by the Poisson equation for the potential

$$\Delta\varphi = en/\varepsilon_0, \tag{3}$$

the equation of continuity

$$\operatorname{div} \mathbf{J} = 0, \tag{4}$$

and the conservation of energy

$$mc^2(\gamma - 1) - e\varphi = W. \tag{5}$$

These equations are equally applicable to the diode region and to the drift space (at least, in one dimension). Consequently we can expect that the drift space will be simply a reflection of the diode about the plane of the anode foil. This means that at a distance $d \approx d'$ a virtual cathode is formed which has the same potential as the real cathode. The anode and the virtual cathode together can be called a virtual diode.[5)]

At this stage we can already see that, whereas in a real diode negatively charged particles (electrons) are accelerated in the positive direction of the $x$ axis, in a virtual diode positively charged particles (ions) are accelerated in the same direction. Although there is no exact proof, we would like to extend the results of the one-dimensional discussion to the two-dimensional case, which is close to reality, and to state that the drift space is the image of the diode region, possibly with a change of spatial scale (mainly in the radial direction). Then it is easy to understand the cause of beam suppression. Since the beam is produced at the cathode with zero velocity, it must stop at the virtual cathode.

Next we can estimate the order of magnitude of the fields of the electron beam, which in the last analysis provide the acceleration of the ions. These fields must be of the same order as the field in the diode. If we use voltages of the order of 1 MV and anode–cathode gaps of about 1 cm, we obtain an electric field strength in the drift space of the order $10^6$ V/cm.

In speaking about reflection, it is necessary in addition to point out in what direction the electrons are moving after stopping at the virtual cathode. Two cases present special interest. In the first case, in which a very strong longitudinal magnetic field is applied, the electrons are tied to the lines of force, i.e., they can move only in the longitudinal direction. In this case the electrons are reflected backward through the anode foil into the diode region, increasing the space charge in the diode and the drift space. After multiple reflections they lose energy as the result of scattering in the anode foil and eventually are captured by the anode. In the second case, in which there is no external magnetic field, most of the electrons are scattered on the walls of the drift chamber after reflection from the two-dimensional potential hump created by the virtual cathode. Accumulation of additional space charge in the region between the real and virtual cathodes does not occur. Since most experiments have been carried out in the absence of a magnetic field, it is the second case which presents the main interest for us.

Before turning to a quantitative analysis of electrostatic beam suppression, let us note the further development of the ionization-front model. Beam suppression occurs also in the presence of an initially neutral gas. However, the gas can be ionized by the electrons and by the ions accelerated in the stationary potential well near the anode. The ionization leads to neutralization of the negative space charge of the beam, removing in this way the cause of the suppression. The beam front, i.e., the virtual cathode, begins to move with a velocity determined by the simple relation

$$v_f = d/\tau_{ef}, \tag{6}$$

where $d$ is the size of the beam-front region and $\tau_{ef}$ is the effective ionization time.

Thus, we have obtained a simple and extremely approximate picture according to which the virtual diode accelerates ions and in addition moves in the same direction with them, thereby increasing their energy to values which exceed the applied voltage.

Let us turn now to a quantitative description of beam suppression. We shall assume that a uniform beam with radius $a$ and current $I$ is moving in a drift tube of radius $R$. Then, solving the Poisson equation for the potential on the axis, we obtain

$$\varphi(r=0) = (-I/4\pi\varepsilon_0 c\beta)(1 + 2\ln R/a), \tag{7}$$

where the total current $I$ is given by the expression

$$I = \pi a^2 en\beta c; \tag{8}$$

[5)] We note in passing that the reflection principle has been applied to the so-called reflection triodes used for direct acceleration of ions.[70]

$\beta c$ and $n$ are the electron velocity and beam density, respectively.

We shall assume that the drift tube is at zero potential. Equation (7) shows that the electron beam produces a sagging of the potential. For the injected electrons to be propagated, it is obviously necessary that the sagging of the potential be less than the accelerating voltage on the diode. Therefore, equating the potential on the axis to

$$\varphi = -U = -(mc^2/e)(\gamma - 1), \tag{9}$$

thereby postulating that the electrons lose all of their kinetic energy, we obtain from Eq. (7) a crude estimate for the maximum current which can be transported through the drift tube:

$$I_c' = I_0 \beta (\gamma - 1)/(1 + 2 \ln R/a). \tag{10}$$

Here we have used the value of $U$ from Eq. (9), and $I_0 = 4\pi\varepsilon_0 mc^3/e \approx 17$ kA is the natural unit of current. The current determined by Eq. (10) is called the electrostatic limiting current.

A more rigorous analysis taking into account the slowing down of the electrons was carried out by Bogdankevich and Rukhadze.[71] Their results can be reduced to the interpolation formula

$$I_e = I_0 (\gamma^{2/3} - 1)^{3/2}/(1 + 2 \ln R/a) \tag{11}$$

for the limiting current. This expression for the current (without the prime) is what we shall use in the remainder of the article unless otherwise stated. The two values for the limiting current are shown in Fig. 38 as a function of the injected electron energy. A comparison shows that always $I_e' > I_e$, and for the highly relativistic case $I_e' \approx I_e$, whereas for nonrelativistic energies these values differ by about a factor of two. Typical values of the limiting current $I_e$ lie in the range from 5 to 150 kA (for details see Table I).

We shall assume now that the current $I$ injected through the anode foil into the drift space exceeds the limiting value: $I > I_e$. It is clear that such a current cannot propagate along the tube.

It is useful to investigate first only the longitudinal suppression of the beam. For this purpose we shall assume that the injected current exceeds the limiting current sufficiently that the depth of penetration $d$ is substantially less than the beam radius $a$.

If we neglect for the time being the slowing down of the electrons in the field of the space charge and assume that there is simply reflection from the virtual cathode at $x = d$, then, integrating the Poisson equation with the boundary conditions $\varphi(x=0) = 0$, $d\varphi/dx(x \geq d) = 0$, we obtain

$$\varphi(x) = (-en/2\varepsilon_0)[d^2 - (x-d)^2]. \tag{12}$$

This expression gives the potential in the space between the anode and the virtual cathode (in the approximation of constant velocity). Beyond the virtual cathode the potential has a constant value

$$\varphi = (-en/2\varepsilon_0) d^2. \tag{13}$$

In order that reflection occur, this potential must exceed the kinetic energy of the injected electrons. Assuming equality, we find the position of the virtual cathode

$$d = \sqrt{\frac{2\varepsilon_0}{e^2 n} mc^2 (\gamma - 1)} = \sqrt{2}\, \frac{c}{\omega_b} \sqrt{\gamma - 1}. \tag{14}$$

In the last expression we have introduced the plasma frequency of the beam

$$\omega_b = (e^2 n/\varepsilon_0 m)^{1/2}.$$

Expressing the beam density in terms of the current density $J$, we can obtain an expression for $d$ in another useful form

$$d = \sqrt{2\varepsilon_0 \frac{mc^3}{e} \frac{\beta(\gamma - 1)}{J}}. \tag{15}$$

This formula shows that the depth of penetration of the beam increases approximately[6)] as the square root of the energy and falls off inversely in proportion to the square root of the current density.

The one-dimensional discussion is valid only for $d \ll a$. Assuming that the beam is uniform over its radius, we have $J = I/\pi a^2$. Taking into account Eq. (15), the condition $d \ll a$ is equivalent to the inequality $I \gg I_0 \beta(\gamma - 1)/4$, which is none other than the condition of strong excess of the injected current over the limiting current for reasonable ratios $R/a$.

This simple method of finding the penetration depth is easily generalized for a chamber of finite length $L$. In this case we must solve Poisson's equation with the additional boundary condition $\varphi(L) = 0$. If the current is above the critical value (see below), a virtual cathode appears which separates the drift space into two regions. The first region (near the anode) contains the injected electrons (the current $I$) and the electrons reflected from the virtual cathode (the reflected current $I_-$), whereas in the second region there are present only electrons which have passed through the virtual cathode (and which form the transmitted current $I_+$). The law of conservation of current $I = I_+ + I_-$ removes one of the currents $I_\pm$ from consideration. The following two questions are of interest: for a given injected current $I$, energy $mc^2(\gamma - 1)$, and length $L$, to determine (a) the transmitted current $I_+$ as a function of $I$ and (b) the position of the virtual cathode $d$.

The critical current density is found by again equating

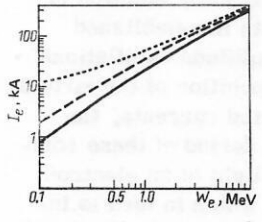


FIG. 38. Electrostatic limiting current as a function of electron energy for $R = a$: the solid curve corresponds to Eq. (11), and the dashed curve to Eq. (10). For comparison we have shown the Alfven–Lawson limiting current, which corresponds to magnetic suppression of the beam (dotted line).

[6)] Neglecting the weak dependence on $\beta$.

the minimum potential to the kinetic energy of the injected electrons.[7)] Since at a current below the limiting value for $x = L/2$ the potential is minimal, we can use the relation (15) with $d = L/2$ and $J = 2J_e$, since the reflection which is taken into account in Eq. (15) is absent in this case, and we obtain

$$J_e = (2I_0/\pi)\,\beta\,(\gamma-1)/L^2. \tag{16}$$

For $J < J_e$ the transmitted current is equal to the injected current $J_+ = J$. For $J > J_e$ we have the relations

$$2J = (1/d^2 + 1/(L-d)^2)\,J_e L^2/4 \tag{17}$$

and

$$J_+ = \frac{L^2}{(L-d)^2}\frac{J_e}{4}, \tag{18}$$

which permit $d$ and $J_+$ to be expressed in terms of $J$, $L$, and $\gamma$.

The approximate solution has the form

$$\left.\begin{aligned} &d \approx (L/2)\,[1-(1/\sqrt{3})\sqrt{J/J_e-1}] \quad \text{for } J/J_e-1 \ll 1;\\ &J_+ = J_e\,[1-(2/\sqrt{3})\sqrt{J/J_e-1}] \quad \text{(weak-supercriticality)} \end{aligned}\right\} \tag{19}$$

and

$$\left.\begin{aligned} &d \approx L\sqrt{J_e/8J} \quad \text{for } J/J_e \gg 1;\\ &J_+ \approx J_e/4 \quad \text{(weak-supercriticality)}. \end{aligned}\right\} \tag{20}$$

As can be seen from Eq. (19), for $J > J_e$ there is a rapid decrease of the transmitted current and of the distance from the anode to the minimum of the potential. For very high currents the penetration depth (20) coincides with the value (15) obtained previously. It is interesting to note that the transmitted current approaches a nonzero limit for injected currents substantially exceeding the limiting value. This is physically clear from the following considerations. In the supercritical case the drift region consists essentially of two virtual diodes of opposite polarity working in the space-charge limited regime. In the first diode ($0 < x < d$) the space charge includes the reflected electrons and is determined by the sum $J + J_- = 2J - J_+$, while in the second diode the only current flowing is the transmitted current $J_+$. Now using the Child–Langmuir law (see, for example, Ref. 74) for both diodes, in the ultrarelativistic approximation (constant velocities) we obtain relations (17) and (18). The critical current $J_e$ is accordingly the Child–Langmuir current for the voltage corresponding to the energy of the injected beam and a diode gap equal to half the length of the drift chamber. With a significant increase of the injected current, $d$ decreases to zero and the length of the second diode approaches $L$. While the exact expression for the Child–Langmuir current is proportional to $1/L^2$, the limiting value of the transmitted current is actually equal to 25% of the critical value. The exact theory has been developed by Voronin *et al.*[75] As was expected, only the dependence on the energy changes; for example, for $d$ instead of Eq. (15) we obtain[76]:

$$d_0 = \frac{1}{2}\sqrt{\frac{I_0}{4\pi J}}\int_1^{\gamma} ds\,(s^2-1)^{-1/4} \approx \sqrt{\frac{I_0}{4\pi J}}\,(\gamma^{2/3}-1)^{3/4}, \tag{21}$$

where in the last expression the elliptic integral is replaced by the approximate value.

Thus, inclusion of the slowing down of the electrons reduces to replacement of $\beta(\gamma-1)$ by the approximate value $(\gamma^{2/3}-1)^{3/2}$, as in the case of cylindrical geometry [see Eqs. (10) and (11)]. The relations (17) and (18) have been checked experimentally by Miller and Straw.[77] They used a beam with parameters 20 kA, 2 MeV, 40 nsec, and a front duration 6–10 nsec in a magnetic guide field of strength up to 7.8 kG. Good agreement was found between theory and experiment. The presence of a characteristic rapid decrease of the transmitted current on exceeding the critical value was confirmed within the experimental error. Values of $d_0$ for the experiments on ion acceleration discussed in their work can be found in Table I.

It is appropriate to make here some remarks of a general nature. Electrons which have been reflected from the virtual cathode will return to the diode and again be accelerated in the drift space until their loss as the result of escape in the radial direction or scattering in the anode foil. Such oscillating electron bunches have been studied by several authors (see Refs. 78 and 79 and references cited therein, and also Refs. 80 and 81). We note again that a systematic theory of injection of electron beams even in the simplest cases must include the diode region in the discussion. The properties of the anode foil particularly affect the stationary state. For simplicity we shall assume that the anode is semi-impenetrable, i.e., transparent for electrons moving from the diode to the drift space, but absorbing electrons reflected backward (see also the article by Ryutov[81]).

Up to this point we have considered only stationary states in the injection problem. It is important, however, to have information also on the time behavior of the quantities of interest. It was clear some time ago that construction of an analytic nonstationary theory is practically impossible and that it is necessary to resort to numerical modeling by computer (see, for example, Ref. 82 and references therein).

A thorough study of the relation between the stationary and time-dependent currents in the nonrelativistic case was carried out by Birdsall *et al.*[72] It turned out that in the presence of a virtual cathode the static solution is unstable[8)] and a quasistationary state is established which is characterized by large-amplitude oscillations of all quantities (the potential, the position of the virtual cathode, the transmitted and reflected currents, the charge density, and so forth). The period of these solutions is determined by the time of flight of an electron reflected from the virtual cathode, which in turn is inversely proportional to the plasma frequency $\omega_b$ of the

[7)] Actually the situation is somewhat more complicated. If a virtual cathode is not formed, then there are two stationary solutions (see, for example, Birdsall and Bridges[72]) for the same set of initial parameters $J$, $L$, $\gamma$. The solution with the greater minimum velocity of the particles gives a limiting current which is twice the value (16). However, this solution is unstable.[73]

[8)] As we have already mentioned, the stability of the static solution was investigated rather recently by Pashchenko *et al.*[73]

beam.

The occurrence of oscillations can be understood in the following way. At the initial moment the electrons pass freely into the drift space. Charge accumulates and produces a sag of the potential. Eventually the main part of the electrons (except for the first ones) are reflected from the potential barrier and the drift space is discharged, giving a current back into the diode. The potential rises, the electrons again can penetrate into the drift space, and the process is periodically repeated. These oscillations permit explanation of the penetrability of the virtual cathode, which is hardly understandable in the framework of the static approximation, in view of the fact that in the static case the initial conditions for each of the electrons are identical. The relativistic case has been discussed by Poukey and Rostoker[76] and also investigated in detail by Hantzsche.[83,84] Qualitatively the same picture is observed.

The problem of injection can be investigated analytically (in the one-dimensional case) up to the moment of the first crossing of the trajectories of particles (reflected and entering) or incidence of an electron onto an electrode.[9)]

The most interesting results are as follows: 1) the depth of the potential well can be $\delta$ times greater than the value corresponding to the kinetic energy of the injected electrons; 2) the deepening coefficient of the well $\delta$ is determined by the time dependence of the injected current. For a current step (zero-duration front) the coefficient $\delta$ changes from 3.0 to 2.14 on change of the energy from nonrelativistic to ultrarelativistic values. On the other hand, if the current rises as $(t/t_r)^\nu$, the enhancement coefficient does not depend on $t_r$, a result which for the case $\nu = 1$ was obtained also by Olson,[28] and increases with increase of $\nu$, but drops with increase of energy. The greatest value $\delta = 3.92$ was obtained for $\nu \to \infty$ and nonrelativistic energies.

In order to trace the behavior of the system at times when the analytic hydrodynamical solution is no longer applicable (as the result of the appearance of multiple fluxes), several numerical studies of the injection problem have been carried out, including the following: a one-dimensional model with an infinitely long drift chamber,[76] with a finite length, the 1.5-dimensional model (an external longitudinal magnetic field of infinite strength and cylindrical geometry of the fields) of Kolomenskiĭ and Novitskiĭ,[72,85] the calculation of Poukey and Olson[86] in a two-dimensional case which is close to reality, and also two-dimensional modeling of injection of a very thin beam ($R \gg a$) into vacuum.[87] Some results of computer calculations are given also in Ref. 26.

The most important results of these studies are as follows: 1) on the whole, all quantities undergo strong oscillations as in the nonrelativistic case; 2) the amplitude of the oscillations decreases significantly with increase of the spread in longitudinal velocity; 3) in all cases except the one-dimensional case with an infinite drift chamber, the sagging of the potential $\delta$ is at the most 1.5 and never reaches the analytic values mentioned above.

We arrive at the conclusion that the attractive idea of associating the observed high energies of accelerated ions with deepening of the potential well (as a result of the nonstationary nature of the injection process), as was done in the theory of Olson,[28] must be rejected.

To combine the case of a purely radial dependence of the potential, in which the limiting current is given by Eq. (11), and the longitudinal discussion which leads to Eq. (21) for the depth of penetration of the beam, it is useful to find an exact solution of the Poisson equation in terms of the Green's function for a cylindrical chamber of length $L$ and radius $R$ which is at zero potential. For an axially symmetric distribution of charge in the chamber we have

$$\varphi(r, x) = \int_0^R dr' r' \int_0^L dx' G(r', x'; r, x)\, \rho(r', x'), \tag{22}$$

where $\rho$ is the charge density divided by $\varepsilon_0$, and (see Ref. 88)

$$G(r', x'; r, x) = \frac{2}{R} \sum_{n=1}^{\infty} \frac{J_0(\lambda_n r/R)\, J_0(\lambda_n r'/R)}{\lambda_n J_1^2(\lambda_n)} \times \frac{\operatorname{sh}\{\lambda_n [L - \max(x, x')]/R\} \operatorname{sh}[\lambda_n \min(x, x')/R]}{\operatorname{sh}[\lambda_n L/R]}, \tag{23}$$

where $J_0$ and $J_1$ are Bessel functions of first order and $\lambda_n (n = 1, 2, \ldots)$ are the zeros of $J_0[J_0(\lambda_n) = 0]$. If the chamber is sufficiently long ($\lambda_1 L/R \gg 1$, i.e., $L/R \gg 1/2.4$), the factor with the hyperbolic sines in Eq. (23) is simplified to the form

$$(\exp[-\lambda_n |x + x'|/R] - \exp[-\lambda_n |x - x'|/R])/2. \tag{24}$$

This expression shows that the potential produced by the charge falls off exponentially in the longitudinal ($x$) direction. At a distance along the axis equal to about $2R$, the field amounts to less than 1% of the maximum value. It follows from this that: 1) the influence of the end wall (at $x = L$) can be neglected if $L > 2R$; 2) the potential well of a beam which is blocked at a distance $x = d_0$ from the entrance plane has an axial extent of the order of the drift-tube diameter.

It is easy to obtain an approximate expression for the limiting current which can pass through a chamber of finite dimensions, assuming the beam to be uniform, nelgecting the slowing down, and equating the potential energy at the center of the system ($r = 0, x = L/2$) to the injection energy. We will not give this expression here but will recall that Miller and Straw[24,41] calculated the limiting current and found satisfactory agreement with experimental data on ion acceleration in the presence of a movable end wall as shown in Fig. 20. It is clear that if the drift chamber becomes shorter, the limiting current increases and if in this case the injected current turns out to be lower, then the suppression does not occur and the accelerated ions should not be observed. This was confirmed experimentally. In ex-

[9)] Use of Lagrangian variables permits us to find a very simple expression for the field strength as a function of the initial position of the particle considered, but only up to the moment of time when one of the events mentioned occurs.

periments on ion acceleration usually $R \ll L$, so that there is no effect of the end wall on the critical current.

Let us consider the following important question. Let $L \to \infty$ and let a current below the critical value $I < I_e$ be injected, where $I_e$ is the limiting current for radial boundaries. Obviously there is no virtual cathode in this case. Now let $I$ approach $I_e$ and go through this value. In this process a virtual cathode must be formed, initially at a large distance from the point of injection, and then gradually approaching it. Thus, the problem consists of determining the position of the virtual cathode $d$ as a function of the ratio $I/I_e$. Since this question has not been discussed in the literature, we have made a crude estimate,[10] proceeding in analogy with the one-dimensional model with Eqs. (17) and (18), and have obtained the result

$$I_+/I \approx (1-\exp[-2{,}4d/R])^2. \tag{25}$$

Here $I_+$ is the current flowing beyond the virtual cathode. This formula is valid for $d \gg R$, i.e., when almost all the injected current can pass.

There are no reasons to assume further that the current $I_+$ is not equal to the limiting value $I_e$ which was determined for the region far from the diode, so that we have

$$2{,}4d/R = -\ln[1-(I_e/I)^{1/2}] \text{ for } I_e < I. \tag{26}$$

This expression shows that the position of the virtual cathode is very sensitive to the amount $\delta I$ by which the injected current exceeds the critical value. Then, for strong supercriticality $I \gg I_e$, we obtain the dependence $d \sim I^{-1/2}$ found in the one-dimensional case for the penetration depth [see Eqs. (15) and (21)], although strictly speaking the applicability of Eq. (26) is limited to weak supercriticality.

The suppression of a beam on injection into vacuum or an initially neutral gas has been well established experimentally (see Figs. 8 and 9). More detailed information on the trajectories of the beam electrons in the absence of an external magnetic field, obtained by numerical modeling, is given in Refs. 86 and 87. These results show that after formation of a virtual cathode on the system axis, the electrons move preferentially along a radius to the walls of the chamber (the beam has a high divergence), and only an insignificant number of particles are reflected backwards or penetrate through the virtual cathode. Thus, in the suppression stage the beam is a "bugle" with a radius which changes from $a'$ to $R$ in a length $d$. The minimum of the potential is at a distance somewhat less than $d$. Beyond the minimum the potential exponentially approaches zero (in a characteristic length equal approximately to $2R$ [see Eq. (24)]. Since usually $2R > d$, the potential well has a very steep fall and a show rise in the direction of motion of the beam. For $d \ll 2R$, i.e., for strong supercriticality, the distribution of the potential along the axis recalls a step.

[10] This question will be discussed in detail in another article by the authors.

As was mentioned previously, with passage of time the beam front begins to move in the direction of the electron flow, when the initially neutral gas is ionized by the beam electrons. Details of the ionization process are discussed below. Here, however, we shall discuss the influence of the partially ionized gas on the suppression mechanism, i.e., we shall find the critical current and the penetration depth in the case in which the space charge of the beam is compensated to a relative value $\varkappa = n_i/n_e$ by fixed positive ions.

If we neglect the slowing down of the beam, we have the same problem as in the absence of an ion background with the only difference that the charge density $\rho$ in Poisson's equation must be replaced by $(1-\varkappa)\rho$. If the charge density is proportional to the current, it is necessary to replace $I$ and $J$ by $I(1-\varkappa)$ and $J(1-\varkappa)$, respectively. Thus, for the penetration depth in this approximation we have

$$d = d_0/\sqrt{1-\varkappa}, \tag{27}$$

and the critical current $I_e$ increases to a value

$$I_e = I_0 \frac{(\gamma^{2/3}-1)^{3/2}}{1+2\ln R/a} \frac{1}{1-\varkappa}. \tag{28}$$

If the space charge is completely compensated ($\varkappa = 1$), obviously there will be no electrostatic suppression. However, in this case the magnetic field of the beam leads to pinching of the beam, which prevents its propagation if the current exceeds the well known Alfven–Lawson limit[89]:

$$I_A = I_0 \beta\gamma. \tag{29}$$

It is possible that the degree of neutralization is such that the electrostatic repulsion is completely compensated by the magnetic attraction. The condition of such equilibrium of the radial forces usually is taken to be Eq. (1). One of the authors of the present article has shown[90,91] that the degree of charge compensation $\varkappa$ is not constant over the beam cross section, but is given by the formula

$$\varkappa(r) = \left(1 + \frac{r}{4}\frac{d}{dr}\right)\frac{1}{\gamma^2(r)}, \tag{30}$$

where $\gamma(r)$ is the relativistic factor, which depends on the radius. If $\gamma(r)$ increases with the radius $r$ (which usually happens), then $\varkappa(r)$ is less than $1/\gamma^2(r)$.

The exact value of the limiting current for such equilibrium is given by the expression

$$I_A^{FN} = I_0\sqrt{\gamma_a^2-1} = I_0\beta_a\gamma_a. \tag{31}$$

In this relation it is easy to see the Alfven–Lawson current for the dynamical quantities $\gamma$ and $\beta$ taken at the edge of the beam. The exact expression (31) gives a larger value for the limiting current than the approximate expression (28) with $\varkappa = 1/\gamma^2$. For energies in the range 0.5–2 MeV which present interest, these values differ by about a factor of two. In what follows we shall use Eqs. (27) and (28), since they are simpler.

*Motion of ions in the head part of the beam.* Here we shall investigate in detail the motion of ions in the electric field in the beam front (the head part). We shall assume the existence of a potential well which is open on the beam-front side, which for a period of time

$T_1$ moves with constant velocity $v_{f1}$, after which the velocity changes discontinuously to a value $v_{f2}$. The existence of two velocities is clearly traced in experiments (see Sec. 2) and also is a consequence of our theory of motion of the beam front which is set forth below.

The assumption of a drop in the potential (a well open on one side) simplifies the calculation (it is possible to neglect the slowing down of the ions) and is justified by the final results. The potential decreases inside the region of the beam front of length $d$ from $e\varphi = 0$ to $e\varphi = -W_0 = mc^2(\gamma - 1)\delta$ and is constant beyond the front. The factor $\delta$ describes the deepening of the potential due to transient effects. The constancy of the potential beyond the beam front means that we are assuming complete neutralization of the space charge (and high conductivity) beyond the front, and that the rear end of the beam in the chamber is at the anode potential. As a result of the motion of the ions, the distribution of the space charge of the beam changes in a complicated way. Even in the one-dimensional case it is difficult to obtain a self-consistent solution of this problem. We shall make several radical simplifications and shall assume that in the head part of the beam, i.e., in the region of partial neutralization:

a) the potential decreases linearly, $\Delta\varphi = W_0/e$; b) the electron density $n_e$ is constant; c) the ion density $n_i$ is constant.

With these assumptions the acceleration process can be described qualitatively as follows. Ions are produced with zero initial velocity and are accelerated at the potential drop. Depending on the front velocity $v_{f1}$ the ions can escape forward beyond the front, in which case their maximum velocity is equal to twice the front velocity; for a very high velocity $v_{f1}$ the acceleration is interrupted and the ions escape beyond the rear edge of the head part of the beam. The particles can be divided into two groups depending on their energy: in the first group are particles with low energy with a maximum value $W_0$: the second group consists of particles with high energy with a maximum value four times the electron injection energy (for $\delta = 1$).

When the velocity reaches its second value, the process just described can be repeated and the group of particles with high energy produced in the first step of acceleration can be accelerated to the quadrupled velocity $v_{f1}$ and accordingly to an energy 16 times greater than the injection energy $W_0$.

Let us turn now to a quantitative analysis. We designate by $\xi$ the coordinate of the ion in the system moving together with the front. Then the position of an ion with a charge state $Z$ and mass $M$ which is at rest at the initial moment is given by the formula[11)]

$$\xi = \xi_0 - v_f t + gt^2/2, \tag{32}$$

where

$$g = \frac{Z_e E_0}{M} = \frac{ZW_0}{Md} \tag{33}$$

is the acceleration; $\xi_0$ is the initial coordinate of the ion. Introducing the dimensionless quantities

$$\lambda = \xi/d, \quad 0 \leqslant \lambda \leqslant 1; \tag{34}$$

$$\alpha = v_f/(2dg)^{1/2}; \quad (2dg)^{1/2} = c\,[(2m/M)\,Z\,(\gamma - 1)]^{1/2}; \tag{35}$$

$$\theta = t/(2d/g)^{1/2}; \quad (2d/g)^{1/2} = (d/c)\,\{2M/[mZ\,(\gamma - 1)]\}^{1/2}, \tag{36}$$

we rewrite Eq. (32) in the form

$$\lambda = \lambda_0 - 2\alpha\theta + \theta^2. \tag{37}$$

The acceleration of the ion in the space-charge field is terminated when it passes the point $\lambda = 0$ (backward escape of the ion) or $\Lambda = 1$ (escape beyond the forward front). The time of escape is

$$\tau_- = \alpha - \sqrt{\alpha^2 - \lambda_0}. \tag{38}$$

This is valid only for ions with an initial coordinate lying in the interval $0 \leqslant \lambda_0 < \alpha^2$. During this time the ion acquires an energy (in units of $W_0 Z$ in the laboratory system)

$$\varepsilon_- = (\alpha - \sqrt{\alpha^2 - \lambda_0})^2 = \tau_-^2. \tag{39}$$

For ions with an initial coordinate lying in the interval $\alpha^2 < \lambda_0 \leqslant 1$, we have

$$\tau_+ = \alpha + \sqrt{\alpha^2 + 1 - \lambda_0} \tag{40}$$

and

$$\varepsilon_+ = (\alpha + \sqrt{\alpha^2 + 1 - \lambda_0})^2 = \tau_+^2. \tag{41}$$

It follows from Eq. (39) that the energy of the slow ions lies in the range $0 \leqslant \varepsilon_- \leqslant \lambda_0 \leqslant 1$, i.e., the energy acquired by them per unit charge does not exceed the energy of the electron beam. The energy of the fast ions, as can be seen from Eq. (41), lies in the interval $(1 - \lambda_0) < \varepsilon_+ < (1 + \sqrt{\lambda_0})^2 \leqslant 4$, i.e., it can reach four times the electron energy, as was noted previously.

We note that the group of fast ions appears only in the case in which the front velocity $\alpha$ is less than unity. The equality $\alpha = 1$ corresponds to coincidence of the front velocity and the velocity $v_i$ of the ion whose energy per unit charge is equal to the electron energy

$$Mv_i^2/2 = ZW_0. \tag{42}$$

The average time $\mu$ which the ion spends inside the head part of the beam depends on the velocity $\alpha$. Integrating $\tau_-$ and $\tau_+$ over $\lambda_0$ within appropriate limits on the assumption that the ions are produced uniformly inside the head part of the beam, we arrive at the expression

$$\mu(\alpha) = \int_0^1 d\lambda_0 \tau = \int_0^{\alpha^2} d\lambda_0 \tau_- + \int_{\alpha^2}^1 d\lambda_0 \tau_+$$

$$= \begin{cases} \alpha + \frac{2}{3}(1 - 2\alpha^3) & 0 \leqslant \alpha < 1; \\ \alpha + \frac{2}{3}(\alpha^2 - 1)^{3/2} - \frac{2}{3}\alpha^3, & \alpha > 1. \end{cases} \tag{43}$$

This function is shown in Fig. 39. We note for comparison that the average time in the absence of an electric field (the free flight time) is $1/4\alpha$. It follows from this that for $\alpha > 0.274$ the ions remain longer in the head part of the beam in the presence of an electric field than without it (accumulation), while for $\alpha < 0.274$ the

[11)] The nonrelativistic discussion of the motion of the ions is valid, since even for protons with energy 10 MeV we have $v/c \approx 0.02$.

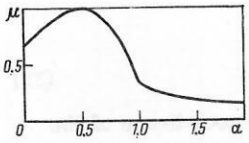


FIG. 39. Average time $\mu$ spent by ions inside the head part of the beam as a function of the dimensionless velocity of the beam front $\alpha$. See Eqs. (35), (36), and (43).

ions are expelled by the field and their density decreases. As can be seen from Eq. (43), in the limiting case of high velocities, $\mu$ approaches $1/4\alpha$.

Let us turn now to the ion spectra predicted by the acceleration theory discussed above. It turns out that the velocity spectrum is more suitable for study than the energy spectrum. A general formula for the momentum spectrum can easily be obtained from the conservation of energy.

In the system of coordinates moving together with the beam front, the energy conservation law has the form

$$W' = Mv'^2/2 + Ze\varphi(\xi) = \text{const}. \tag{44}$$

At the moment of formation of an ion at the point $\xi_0$ we have $v' = -v_f$. When it leaves the head part of the beam, outdistancing it ($v_+$) or lagging behind it ($v_-$), the velocity is determined by the formulas

$$v_f'^2 = v_f^2 + (2Ze/M)(U + \varphi(\xi_0)); \tag{45}$$

$$v_-'^2 = v_+^2 + (2Ze/M)\varphi(\xi_0). \tag{46}$$

We note that the velocity $v_+$ is positive and $v_-$ is negative. The velocities in the laboratory system are obtained by addition to $v_\pm$ of the front velocity,

$$v_+ = v_f + \sqrt{v_f^2 + (2Ze/M)(U + \varphi(\xi_0))}; \tag{47}$$

$$v_- = v_f - \sqrt{v_f^2 + (2Ze/M)\varphi(\xi_0)}. \tag{48}$$

Then the number of ions $dN$ which appear per unit time outside the head part of the beam with velocity in the interval between $v$ and $v + dv$ is

$$\frac{dN}{dv} = \frac{dN}{d\xi_0}\frac{1}{dv/d\xi_0}. \tag{49}$$

Using Eqs. (47) and (48), we find the derivatives

$$\frac{dv_\pm}{d\xi_0} = -\frac{(Ze/M)E}{v_\pm - v_f} = \frac{(Ze/M)E}{v_f - v_\pm}, \tag{50}$$

where the electric field strength $E = -\partial\varphi/\partial\xi_0$ is positive. Since $v_f < v_+$, we have $dv_+/d\xi_0 < 0$, i.e., particles with smaller initial coordinate $\xi_0$ are accelerated to higher velocities than particles with larger $\xi_0$.

Combining Eqs. (50) and (49) and assuming creation of ions inside the head part of the beam to be equally probable over the length ($dN/d\xi_0 = N/d$), we find

$$\frac{dN}{dv} = N\frac{Mv_f}{Zed}\frac{|1 - v/v_f|}{E(\xi_0)}. \tag{51}$$

Here $\xi_0$ must be expressed in terms of $v$ and $v_f$ by means of Eqs. (47) and (48) and the velocity $v$ coincides with $v_+$ or $v_-$ in the corresponding intervals, which are determined from the energy conservation law [see Eqs. (53) and (54)]. We see the universal dependence of the spectrum on the velocity through $|1 - v/v_f|$, and also on the details of the field structure in the head part of the

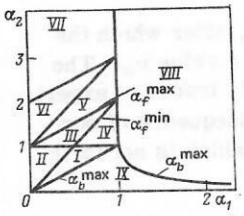


FIG. 40. Regions of the beam-front velocities in two-stage acceleration. We have shown the maximum velocity of ions $\alpha_b^{max}$ which are accelerated but leave the head part through the rear edge in the first stage, and also the maximum and minimum velocities of ions from the high-energy group produced in the first step of acceleration.

beam. Previously we restricted the discussion to the simplest case, assuming the electric field to be constant, $E = W_0/ed$. Substituting the last expression into Eq. (44), we arrive at a dimensionless equation for the spectrum

$$dN/d\alpha = 2N\alpha_1 |1 - \alpha/\alpha_1|, \tag{52}$$

where $\alpha$ is the ion velocity and $\alpha_1$ is the beam-front velocity. The different velocity intervals are shown in Fig. 40. The curve $\alpha_b^{max}$ determines the maximum value of the velocity (plotted along the $\alpha_2$ axis) of an ion belonging to the slow group, while the velocities of ions of the fast group lie between $\alpha_f^{min}$ and $\alpha_f^{max}$. We note that with increase of energy the spectrum of the group of fast ions becomes narrower.

A typical spectrum for $\alpha < 1$ is shown in Fig. 41 (the region V, the dashed line). It should be noted that a linear or even monotonically increasing or falling dependence of $dN/d\alpha$ occurs only for a constant electric field strength; for a variable field strength this dependence has a different nature. However, the grouping of the particle always remains for $\alpha_1 < 1$.

We shall assume that the spectrum of ions for a beam-

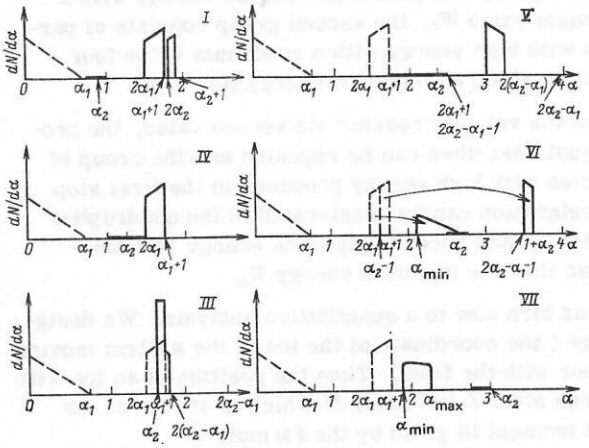


FIG. 41. Ion spectra obtained as the result of two-step acceleration for various regions of beam-front velocity for $\alpha_1 = 0.75$ and various values of $\alpha_2$ (from Fig. 40): dashed lines—spectra produced in the first step; solid lines—pre-acceleration part of the spectrum; the arrows in region VI show the result of the pre-acceleration; the heavy lines on the $\alpha$ axis indicate the interval in $\alpha_2$ corresponding to the selected value $\alpha_1 = 0.75$ (see Fig. 40).

front velocity $\alpha_1$ has been established and that the front velocity has changed discontinuously to a new value $\alpha_2$. There are several possible energy spectra after the second acceleration. In Fig. 40 we have shown the various regions in the $\alpha_1, \alpha_2$ plane. We are interested in those regions in which qualitative and quantitative changes occur in the spectra, and the most interesting regions are those with the maximum ion energy. Typical spectra are shown in Fig. 41 for $\alpha_1 = 0.75$.

Region IX in Fig. 40 is of no interest, since the front velocity is less than the ion velocity before the discontinuity (this region of values is not usually encountered in experiments at constant pressure). In region VIII the front is moving more rapidly than any of the ions accelerated previously. In the first stage of acceleration the ions left the head part of the beam and were lost, since they could not be accelerated in the second stage. This case is practically identical to one-stage acceleration. In regions I and IV the head part of the beam lies between the fast and slow groups of ions in coordinate space and in velocity space; therefore preacceleration does not occur and eventually for low $\alpha_2$ (region I) a new peak of high-energy ions appears, and for high $\alpha_2$ (region IV) the group with low energy is broadened. In regions II and III the beam-front velocity $\alpha_2$ is sufficiently great to pre-accelerate part of the fast ions. For $\alpha_2 < 1$ a peak in the high-energy region again appears, which is due to acceleration of ions from the ion background (their spectrum is similar to the spectrum in region I), in contrast to region III, where eventually one observes a peak of a few preaccelerated ions. In region V all ions of the fast group are pre-accelerated, while in region VI the front velocity is so great that part of them leave the head part of the beam and reach only a maximum velocity equal to $\alpha_2$. The minimum value of the velocity is

$$\alpha_{\min} = \alpha_2 - \sqrt{(\alpha_2 - \alpha_1)^2 - 1}. \tag{53}$$

In this case the maximum energy value is $\varepsilon = 16$. For still larger values of $\alpha_2$ (region VII) all ions leave the head part of the beam and their velocities lie in the interval between $\alpha_{\min}$ and $\alpha_{\max}$,

$$\alpha_{\max} = \alpha_2 - \sqrt{(\alpha_2 - \alpha_1 - 1)^2 - 1}. \tag{54}$$

Thus, the final spectrum contains a low-energy group of ions with velocities less than unity and, possibly, a group of ions with high energy. There may be one or two peaks in energy in the latter. Two peaks are encountered only in the regions I, II, and VI, while in regions III, IV, V, and VII there is only one peak.

*Ionization of the residual gas.* The ions which compensate the space charge of the electron beam are produced in the process of collisions of electrons and alreacy accelerated ions with neutral particles (ionization cross sections $\sigma_e$ and $\sigma_i$, respectively).

As was first pointed out by Alexander *et al.*,[37] in the energy region of interest to us the main role in the ionization process is played by accelerated ions. Subsequently a detailed study of the neutralization process was carried out by Olson. He considered ionization by electron impact, electron avalanche ionization, ionization by ion impact, ion avalanche ionization, charge exchange, preliminary ionization processes, radial escape of secondary electrons, recombination, diffusion, and capture of electrons by neutral particles. It turned out that the principal of these processes are ionization by electron impact, by ion impact, and the appearance of the ion avalanche associated with it. In Fig. 42 we have shown the quantity $\beta S$, which is related to the probability of the various most important processes $\nu$ by the relation $\nu[\text{sec}^{-1}] = \beta S p[\text{Torr}] c$, as a function of energy. The usual cross section is given by the formula $\sigma[\text{cm}^2] = S \cdot 3.54 \times 10^{-16}$. As can be seen from the figure, beginning with about 10 keV ionization by ion impact dominates over ionization by electron impact, and in the region 0.1–0.2 MeV its probability is approximately an order of magnitude higher. In addition, in this region the ionization probabilities are almost independent of energy and we can approximately assume that

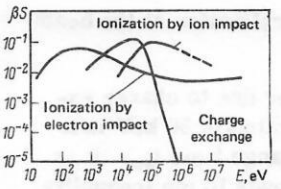


FIG. 42. Normalized reaction probabilities for the principal elementary processes which determine the propagation of an intense relativistic electron beam through a low-pressure gas. Average time of ionization (charge exchange) $\tau[\text{sec}] = (\beta c S p[\text{Torr}])^{-1}$.[92]

$$\nu_e\ [\text{nsec}^{-1}] \approx p/5\ [\text{Torr}] \tag{55}$$

and

$$\nu_i\ [\text{nsec}^{-1}] \approx 2p\ [\text{Torr}]. \tag{56}$$

The ionization time $\tau_i = \nu_{e,i}^{-1}$ of various gases, taken at a pressure 0.1 Torr, on passage through them of electrons and ions of various types is shown in Fig. 43. In what follows we shall make use of Eqs. (55) and (56), since they remain approximately valid for deuterium and helium, i.e., for practically all gases used in experiments on acceleration of ions. Olson called attention to the important role of charge-exchange processes which cut off the acceleration of ions. As can be seen from Fig. 42, ions with energy below 50 keV have a higher probability of exchanging their charge with stationary ions and dropping out of the acceleration process than of being ionized as a consequence of impact (as was shown by Olson, other processes which decrease the charge of ions, such as recombination or electron capture by neutral particles, can be neglected

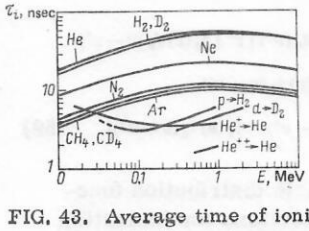


FIG. 43. Average time of ionization of various gases, taken at a pressure 0.1 Torr, in passage through them of electrons and ions of various types.[97-99]

during the entire process of neutralization at the beam front).

In order to overcome the barrier due to charge exchange, a proton must be accelerated to 50 keV in a time $t_a$ less than the charge-exchange time $t_{exc}$. It is easy to show that this condition leads to the inequality

$$E[\text{V/cm}]/p[\text{Torr}] \gtrsim 10^6. \tag{57}$$

We used here $t_{exc} = (c\beta Sp)^{-1}$ and $\beta S \approx 0.1$ from Fig. 42. In order to provide effective acceleration of ions to energies above 50 keV, high electric field strengths and low pressures are necessary. At a typical pressure of 0.1 Torr the field strength must be greater than $10^5$ V/cm. It is usually understood that radial escape of secondary electrons occurs almost instantaneously (in a time of the order $R/c$, which is usually less than 1 nsec) under the influence of the strong electric field which exists right up to complete charge neutralization. After a detailed discussion of the fields, Olson showed that this assumption is justified, and in the low-pressure regime which presents the greatest interest ionization by secondary electrons, like that by electron avalanches, can be neglected. The situation can change substantially only in the case in which radial escape is suppressed by a strong external longitudinal magnetic field.

We included in our model possible effects of preliminary ionization, assuming that partial charge neutralization

$$\varkappa_+ = n_{i+}/n_e \tag{58}$$

occurs in advance of the beam front. Note that we took a positive charge density relative to the density of electrons in the main part of the beam. Previously[37] we assumed that $n_{i+}$ is entirely determined by the number of accelerated ions which are in advance of the beam front. However, Olson[92] showed that preliminary ionization by beam electrons which have escaped forward is also important. As a consequence of the finite rise time, the current in the beam in the leading part of the front is below the critical value [see Eq. (11)], i.e., it can be propagated along the drift tube almost without obstacle. In this way electrons appear which precede the main beam.

As was shown by Olson,[92] other possible effects of previous ionization due to a prepulse of the beam, microwave radiation, or radiation from the anode foil can be neglected.

*Kinetic discussion of the stationary case.* The stationary distribution function of the ions $f_i(v, x)$ is found from the kinetic equation $(\partial/\partial t = 0)$

$$\frac{df_i}{dt} \equiv v\frac{\partial f_i}{\partial x} + \frac{eE(x)}{M}\frac{\partial f_i}{\partial v} = \int dv'\sigma_e(v')\,|\,v'\,|\,f_0(v)f_e(v-v') + \int dv'\sigma_i(v')\,|\,v'\,|\,f_0(v)f_i(v-v') + \int dv'\sigma_{exc}(v')\,|\,v'\,|\,[f_0(v)f_i(v-v') - f_i(v)f_0(v-v')]. \tag{59}$$

Here $f_0(v)$ is the neutral-particle distribution function; $\sigma_i$ and $\sigma_{exc}$ are the cross sections for ionization and charge exchange of an ion, respectively. The first term on the right-hand side describes the ionization of residual-gas atoms by electrons ($\sigma_e$ and $f_e$ are the ionization cross section and the distribution function of the electrons), the second term takes into account ionization by ions, and the last term describes charge-exchange processes.

In writing out Eq. (59) we have neglected collisions in which transfer of energy or momentum occurs, i.e, we assume that the motion of the ions is determined completely by the electric field $E(x)$ (in a sufficiently strong field this is valid). In what follows we shall assume that the gas density is significantly greater than the ion density, so that the variation of $f_0$ can be neglected.

In order to adapt the kinetic equation to the study of our question, we shall make the following assumptions:

1) the neutral-particle distribution function

$$f_0(v) = n_g\delta(v) \tag{60}$$

corresponds to a uniform stationary background;

2) the reaction probabilities $\nu_{i,exc} \equiv n_g\sigma_{i,exc}v$ are approximated by a step function, i.e.,

$$\nu_i(v) = \nu_i\Theta(v-v^*); \tag{61}$$

$$\nu_{exc}(v) = \nu_{exc}\Theta(v^*-v), \tag{62}$$

where $v^*$ is the velocity of protons with energy 50 keV (the charge-exchange barrier);

3) the electric field is assumed constant in the head part of the beam and zero elsewhere.

Using assumptions 1 and 2, we bring the kinetic equation into the form

$$\frac{df_i}{dt} = n_e(x)\nu_e\delta(v) + \nu_i\delta(v)\int_{v^*}^{\infty} dv' f_i(v', x) + \nu_{exc}\delta(v)\int_0^{v^*} dv' f_i(v', x) - \nu_{exc}\Theta(v^*-v)f_i(v, x). \tag{63}$$

Here $n_e(x)$ is the electron density and $\nu_e = n_g\langle\sigma_e v\rangle$ = const is the probability of ionization of the atoms by electrons.

The three terms which contain a $\delta$ function correspond to production of ions with zero initial velocity and disappear for $v > 0$. In the region $0 < v < v^*$ the distribution function is replaced in accordance with the formula

$$df_i/dt = -\nu_{exc}f_i, \tag{64}$$

i.e., $f_i$ decreases exponentially along the particle trajectory. In the case when the electric field is constant, the particle velocity increases linearly with time, so that $f_i$ changes according to an exponential law along the velocity axis up to $v = v^*$. In addition, since we are neglecting all dynamical collisions, the distribution function is determined completely from solution of the equation of motion of one particle.

Thus, in the system moving with the beam front the distribution function is determined by the expression (the subscript i has been omitted)

$$f(x, v) = h\left[x + \frac{1}{2g}(v_f^2 - v^2)\right] \times \begin{cases} \exp\left(-\nu_{exc}\dfrac{v+v_f}{g}\right), & 0 \leqslant v+v_f \leqslant v^*; \\ \exp\left(-\nu_{exc}\dfrac{v^*}{g}\right), & v+v_f > v^*. \end{cases} \tag{65}$$

Here we have set $h(x_0) = f(x_0, v_0 = -v_f, t = 0)$ and have

substituted the initial coordinate $x_0 = x_0(x, v) = x - (v_t^2 - v^2)/2g$. Substituting (65) into (63) and integrating over $v$ in the vicinity $v = -v_t$, we obtain an integral equation for $h(x)$.

Using the dimensionless quantities [for other dimensionless quantities see Eqs. (32)–(36)]

$$\left.\begin{aligned} &\beta = v/H = hgd/(\nu_e N_e); \quad (2gd)^{1/2}; \\ &K(\lambda) = n_e(x)\, d/N_e; \; N_e = \int_0^d n_e(x)\, dx; \; q_{i,\,\mathrm{exc}} = \nu_{i,\,\mathrm{exc}} \sqrt{2d/g} \end{aligned}\right\} \quad (66)$$

and changing the region of integration, we write the integral equation in the form

$$H(\lambda) = K(\lambda) + \int_{G(\lambda,\,\alpha)} d\beta H(\lambda + 2\alpha\beta - \beta^2)$$
$$\times [q_i \exp(-q_{\mathrm{exc}}\beta^*)\,\Theta(\beta - \beta^*) + q_{\mathrm{exc}} \exp(-q_{\mathrm{exc}}\beta')\,\Theta(\beta^* - \beta)], \quad (67)$$

where the region of integration is determined by the formulas

$$\left.\begin{aligned} &G = (0,\ \alpha - \sqrt{\alpha^2 - (1-\lambda)}), \quad \alpha \geqslant 1; \\ &G = \begin{cases} (0,\ \alpha + \sqrt{\lambda}), & 0 \leqslant \lambda \leqslant 1 - \alpha^2; \\ (\alpha,\ \alpha - \sqrt{\alpha^2 - (1-\lambda)}) \text{ and} \\ (\alpha + \sqrt{\alpha^2 - (1-\lambda)},\ \alpha + \sqrt{\lambda}); & 1 - \alpha^2 < \lambda \leqslant 1. \end{cases} \end{aligned}\right\} \quad (68)$$

The particles which are in the head part of the beam occupy a phase space equal to $\int_0^1 d\lambda \int_{G(\alpha,\lambda)} d\beta$. This quantity is exactly equal to the average time $\mu(\alpha)$ which the ion spends inside the head part of the beam, which was introduced previously in Eq. (43). In what follows we shall assume $q_i = q_{\mathrm{exc}} \equiv q$, which is a reasonable approximation (see Fig. 42).

Several important quantities are now expressed as follows: the ion density is

$$n_i(x)\, d/N_e = [H(\lambda) - K(\lambda)]/B, \quad (69)$$

the relative number of ions in the head part of the beam is

$$\varkappa \equiv \frac{N_i}{N_e} = \frac{1}{B} \int_0^1 d\lambda\, [H(\lambda) - K(\lambda)], \quad (70)$$

and the current of accelerated ions, i.e., ions which have left the head part through the front, is

$$\left.\begin{aligned} &\frac{J_+}{2N_e\nu_e} = \int_{2\alpha}^{1+\alpha} d\beta\,(\beta - \alpha)\, H(1 + 2\alpha\beta - \beta^2) \\ &\times \begin{cases} \exp(-q\beta,), & 0 \leqslant \beta \leqslant \beta^* \\ \exp(-q\beta^*), & \beta^* < \beta \end{cases} \quad \text{for} \quad \alpha < 1 \\ &\frac{J_+}{2N_e\nu_e} = 0 \quad \text{for} \quad \alpha \geqslant 1. \end{aligned}\right\} \quad (71)$$

The integral equation (67) must be solved together with an additional equation which relates the quantities $\alpha$, $B$, $\varkappa$, and $q$. As was discussed above, the front velocity is

$$v_f = d\nu_{\mathrm{ef}},$$

where $d$ is the depth of penetration of the electron beam in the presence of partial charge neutralization,

$$d = d_0/\sqrt{1 - \varkappa},$$

and $\nu_{ef}$ is the combined probability of ionization by electrons and ions:

$$\nu_{\mathrm{ef}} = \nu_e + \nu_i \varkappa^f. \quad (72)$$

In the last equation $\varkappa^f N_e$—the number of ions with energy above the charge-exchange barrier $\beta > \beta^*$ (only these ions contribute to the increase of the charge)—is determined by the expression

$$\varkappa^f = \frac{q}{B} \exp(-q\beta^*) \int_0^1 d\lambda \int_{G(\lambda,\,\alpha)} d\beta H(\lambda + 2\alpha\beta - \beta^2)\,\Theta(\beta - \beta^*). \quad (73)$$

In the dimensionless variables Eq. (6) takes the form

$$\alpha = \alpha_0 (1 + B\varkappa^f)/\sqrt{1 - \varkappa}, \quad (74)$$

where we have introduced the parameter

$$\alpha_0 = \nu_e d_c/2, \quad (75)$$

the so-called dimensionless pressure [see Eq. (55)]. Using Eqs. (75), (74), (66), and (36), we find that

$$q = 2\alpha B/(1 + B\varkappa^f). \quad (76)$$

Now $q$ is no longer a free parameter, but must be expressed in terms of $\alpha$, $\varkappa^f$, and $B$ by means of (76). This leads to obvious difficulties, since from the system (73) and (76) a transcendental equation is obtained for $\varkappa^f$.

Thus, a self-consistent discussion of the processes of charge neutralization and beam-front motion leads to an essentially nonlinear integral equation. In principle it is possible to calculate values of $\varkappa$ and $\varkappa^f$ for given $\alpha$, $B$, and $\beta^*$. Substituting the result into Eq. (74), we find the corresponding parameter $\alpha_0$. In the final analysis all stationary quantities depend on the free parameters $B$, $\beta^*$, and $\alpha_0$ and on the electron-density dstribution $K(\lambda)$. In spite of the nonlinearity, the problem is easily solved numerically by an iterative method. In the numerical solution we used the following parameters:

1) in all calculations we set $B = 10$, although in reality there is a weak dependence of $B$ on energy (see Fig. 42);

2) for study of the influence of charge-exchange processes we used three values of the electron energy $W_e$: 50 keV, 1 MeV, and 10 MeV. The corresponding values of $\beta^*$ in this case are 1.0, 0.224, and 0.071 (we note that $\beta^*$ is the velocity of a proton with energy 50 keV expressed in units of the velocity of a proton with energy $W_e$);

3) for the electron density we used two different models: a) uniform ($K = 1$) and b) nonuniform (a peak at the front):

$$K(\lambda) = \begin{cases} 0, & 0 \leqslant \lambda \leqslant 1 - \gamma; \\ 1/\gamma, & 1 - \gamma \leqslant \lambda < 1. \end{cases} \quad (77)$$

The latter is the simplest model of the virtual cathode at the beam front and agrees better with the assumption of a constant value of the electric field strength (these calculations were carried out for a value $\gamma = 0.1$);

4) on change of $\alpha$ (the most important of the parameters) from $5 \times 10^{-3}$ to 10, the parameter $\alpha_0$ changes in the region from $5 \times 10^{-3}$ to 5. Thus, a region with variation of the pressure by three orders of magnitude was covered. Outside of this region of values of $\alpha$ it is possible to use asymptotic formulas (see below).

Before presenting the results of the numerical calcula-

tion, we shall obtain analytic expressions for very low and very high pressures.

For low pressures ($\alpha_0 - 0$) in first order in $\alpha_0$ we have

$$H(\lambda) \approx K(\lambda) + 2\alpha_0 B \int_0^{\sqrt{\lambda}} d\lambda' K(\lambda - \lambda'^2). \tag{78}$$

Thus, the ion density, the degree of neutralization of the space charge, the beam-front velocity, and the accelerated ion current are expressed as follows:

$$\left.\begin{aligned} &n_i d/N_e = 2\alpha_0 \int_0^{\sqrt{\lambda}} d\beta K(\lambda - \beta^2);\\ &\varkappa = 2\alpha_0 \int_0^1 d\lambda \int_0^{\sqrt{\lambda}} d\beta K(\lambda - \beta^2);\\ &\varkappa^f = 2\alpha_0 \int_0^1 d\lambda \int_{\beta^*}^{\sqrt{\lambda}} d\beta K(\lambda - \beta^2);\\ &\alpha = \alpha_0 \left[1 + B\varkappa^f + \frac{1}{2}\varkappa\right];\\ &J_+/N_e v_e = 2\int_0^1 d\beta\beta K(1-\beta^2) = 1. \end{aligned}\right\} \tag{79}$$

For a density chosen in the form (77) we find

$$\left.\begin{aligned} &n_i d/N_e = \frac{2\alpha_0}{\gamma}\sqrt{\lambda - (1-\gamma)}\,\Theta(\lambda - (1-\gamma));\\ &\varkappa = \frac{4}{3}\alpha_0\sqrt{\gamma};\\ &\varkappa^f = \frac{2\alpha_0}{3}\sqrt{\gamma}\left(1 - \frac{\beta^*}{\sqrt{\gamma}}\right)^2\left(2 + \frac{\beta^*}{\sqrt{\gamma}}\right)\Theta(\gamma - \beta^{*2}). \end{aligned}\right\} \tag{80}$$

With increase of $\gamma$ the quantities $\varkappa$ and $\varkappa^f$ increase, so that they reach their greatest values in the uniform case ($\gamma - 1$). The same applies also to $\alpha$. We note that $\varkappa^f = 0$ if $(\beta^*)^2 \geq \gamma$.

For high pressure ($\alpha_0 - \infty$) in lowest order in $1/\alpha_0$, if the additional condition $\varkappa^f = 0$ is satisfied, i.e., for

$$\alpha > (1 + \beta^{*2})/2\beta^*, \tag{81}$$

we find

$$\left.\begin{aligned} &H(\lambda) = K(\lambda) + B\int_\lambda^1 d\lambda' K(\lambda');\quad n_i d/N_e = \int_\lambda^1 d\lambda' K(\lambda');\\ &\varkappa = \int_0^1 d\lambda\lambda K(\lambda) \equiv \langle\lambda\rangle;\quad \alpha = \alpha_0/\sqrt{1 - \langle\lambda\rangle}. \end{aligned}\right\} \tag{82}$$

For the density (77) in this limit

$$\varkappa = 1 - \gamma/2;\ \alpha = \alpha_0\sqrt{2/\gamma}. \tag{83}$$

These quantities reach their maximum values with a sharp peak of the electron density ($\gamma - 0$). The case $\varkappa^f \neq 0$ in which the inequality inverse to (81) is satisfied is more complicated, and we will not give the corresponding expressions here.

Let us return to the beam velocity $\alpha$. For low pressures it follows from Eq. (79) that $\alpha \approx \alpha_0$, while for high pressures we have $\alpha \approx \alpha_0/\sqrt{1 - \langle\lambda\rangle}$. Thus, for both low and high pressures the dependence of the beam-front velocity on the pressure has a simple linear nature. The slope of the curve is higher in the high-pressure region. The degree of charge neutralization $\chi$ in the low-pressure region changes linearly and becomes constant, equal to the "coordinate of the center of mass" of the electron density for high pressures. We arrive at the conclusion that there should exist an intermediate pressure region in which there is a change in the nature of the beam-front propagation. In the intermediate region the equations must be solved numerically. Let us turn to presentation of the results of the numerical solution.

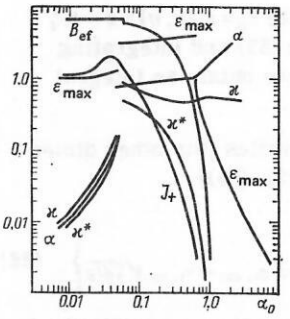


FIG. 44. Various stationary quantities as a function of the dimensionless pressure $\alpha_0$. A solution of the kinetic equation was obtained for $W_e = 1$ MeV and a uniform electron density. Notation: $\alpha$—beam-front velocity, $\varkappa$—average degree of charge neutralization, $\varkappa^f$—the same for ions with energy greater than the charge-exchange barrier; $B_{ef} = B\varkappa^f/\varkappa$ is the effective ionization probability; $J_+$ is the current of ions passing through the leading edge of the head part of the beam; $\varepsilon_{max}$ is the maximum ion energy.

The dependence of the various quantities on pressure is given in Fig. 44. The electron density was chosen to be uniform, and the energy $W_e = 1$ MeV. The most important thing in this plot is the existence of a critical pressure $\alpha_{0cr} = 0.05$ at which certain quantities such as the beam-front velocity and the degree of charge neutralization experience a discontinuity.

Actually, we showed previously[46] in the framework of a simplified model that for a given $\alpha_0 < \alpha_{0cr}$ there are three solutions for $\alpha$. Two of them are stable, and one is unstable. The smallest of them is physically realizable and is shown in the figure. The upper solution is located near the line $\alpha = 1$ and is a continuation of the plateau (see below). This branch is not realized physically. Between these two solutions there is an unstable branch which is a continuation of the smaller solution beyond the point at which $d\alpha/d\alpha_0 = 0$ backward to the axis $\alpha_0 = 0$. Below the critical pressure the beam-front motion is slow, and the degree of charge neutralization is small. Here the asymptotic formulas for low pressures are applicable. The current of accelerated ions, i.e., ions which outdistance the head part of the beam, $J_+$, is one to two times greater than the current for a stationary head part.

In the region from $\alpha_{0cr} = 0.05$ to $\alpha_0 = 0.6$ the beam-front velocity changes little. This region, which covers a range of pressures of more than an order of magnitude, is called the plateau region. Its most important feature, other than the constancy of $\alpha$, is the rapid decrease of the accelerated-ion current. With increase of the pressure the maximum ion energy $\varepsilon_{max}$ increases roughly from two to four.

The pressure at which $\alpha = 1$ and which corresponds to cutoff of acceleration we shall call $\alpha_{0co}$. At a higher pressure $J_+ = 0$, and the maximum ion energy drops

rapidly.

Thus, the stationary acceleration of ions is cut off for $\alpha_0 > \alpha_{0_{co}}$. In the high-pressure region the asymptotic formulas are also applicable for stationary solutions. We emphasize that we are discussing the stationary regime, since (this was mentioned previously) transient effects can lead to a double acceleration of ions, which somewhat changes the picture presented here.

In conclusion we shall briefly discuss the influence of the change of parameters on the results: 1) with change of the energy and (or) uniformity of the electron density, the qualitative nature of the processes described is preserved; 2) if the electron density is nonuniform, the plateau region decreases by a factor of two or more (in the case which we have just discussed in detail the size of the plateau region is the maximum possible); 3) for $\beta^* = 1$ when the energy of all ions is below the barrier for ionic ionization, the ion current remains less than 2% for $\alpha > \alpha_{0_{co}}$. With change of $\alpha$ from 0.3 to 1.0 the plateau is weakly expressed; 4) the critical values of the pressure are as follows:

| Energy | $\alpha_{cr}$ | | $\alpha_{co}$ | |
|---|---|---|---|---|
| | Uniform | Nonuniform | Uniform | Nonuniform |
| 50 keV | 0.09 | — | 0.70 | — |
| 1 MeV | 0.05 | 0.075 | 0.60 | 0.20 |
| 10 MeV | 0.04 | 0.06 | 0.24 | 0.13 |

*Time dependence of the beam-front motion and ion acceleration.* To investigate the behavior of our system with time it is natural to use the kinetic equation (59) with $\partial f/\partial t \neq 0$. Comparison of the results which follow from the stationary model considered above and the results of the simplified first version,[39] which involve averaged values, shows that they are not very different. Therefore we shall consider the time behavior of a system in the framework of the simplified model. The principal one of the time-dependent quantities is the degree of charge neutralization. At the initial moment of time there are no ions, and therefore $\varkappa(0) = 0$. The beam-front velocity, as before, is determined from the formula

$$\alpha = \alpha_0 (1 + B_{ef}\varkappa)/\sqrt{1-\varkappa}, \qquad (74')$$

where

$$B_{ef} = B\varkappa^I/\varkappa, \qquad (84)$$

so that $\alpha(t=0) = \alpha_0$. This means that initially the beam motion is determined by the slow rate of ionization by electrons.

The equation for $\varkappa$ (here $\tau = t/\theta_0$) has the form

$$d\varkappa/d\tau = (2\alpha - \varkappa/\mu(\alpha))\sqrt{1-\varkappa}. \qquad (85)$$

Here the first term describes the production of the ions, and the second describes the flux of ions escaping through the head part of the beam. This flux is equal to the quotient obtained by dividing $\varkappa$ by the average time $\mu(\alpha)$ which the ion spends in the head part.

The function $\mu(\alpha)$ was calculated previously [see Eq. (43)]. From Eq. (85) we obtain the stationarity condition

$$\varkappa = 2\alpha\mu(\alpha). \qquad (86a)$$

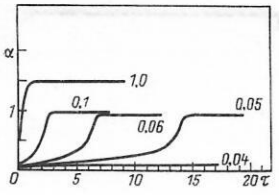


FIG. 45. Beam-front velocity $\alpha$ as a function of time for various values of the dimensionless pressure $\alpha_0$.

It coincides with the condition which is obtained in the kinetic approach, which includes an integral equation. Actually, setting $B=0$, i.e., neglecting ionic ionization and charge-exchange processes and assuming the electron density to be constant, we see that Eq. (86a) follows directly from solution of the kinetic equation [see Eqs. (70), (67), and (68)]. Even for $B=0$ this simple solution with (74′) already contains the most important features of the picture described in the preceding section.

From Eqs. (86a) and (43) it is easy to see also that there is a region $0.5 < \alpha \leq 0.9$ in which $2\alpha\mu(\alpha) > 1$. It is clear that in this region the beam-front velocity cannot be stationary.

The quantity $\mu(\alpha)$ was calculated for $\alpha = \text{const}$, and Eq. (74′) is also suitable in the quasistationary case in which the acceleration $d\alpha/d\tau$ is significantly less than unity. In the present calculations this condition is not satisfied during the entire time interval considered. The violations occur in a very short time interval (at the time of the discontinuity), so that we can neglect their influence.

The results of numerical solution of Eqs. (85) and (74′) with $B_{ef} = 10$ are shown in Figs. 45 and 46 for various pressure values in the plateau region of interest here.

As can be seen from Fig. 45, in the plateau region the beam-front velocity is at first small and remains small for some additional time, but then changes abruptly to a stationary value close to unity. This is the transient behavior of the beam-front velocity from one value to another which we mentioned previously. At low pressures ($\alpha < \alpha_{0_{cr}}$) the velocity remains approximately equal to its initial value $\alpha_0$ (see the curve with $\alpha_0 = 0.04$), and for pressure values corresponding to the cutoff of acceleration in the stationary model the front velocity changes practically instantaneously to

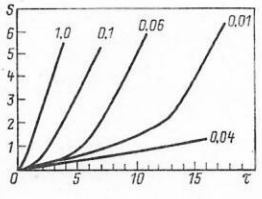


FIG. 46. Path traveled by beam front as a function of time for various values of the parameter $\alpha_0$.

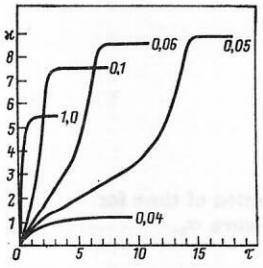


FIG. 47. Average degree of charge neutralization $\varkappa$ as a function of time for various values of the parameter $\alpha_0$.

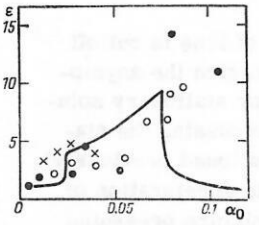

FIG. 49. Maximum ion energy as a function of pressure, and comparison of theoretical results (solid line) and experimental results: ×—Graybill *et al.*[29,30]; ○—Ecker *et al.*[19]; ●—Kolomenskiĭ *et al.*[20,31]; see Figs. 13–15.

its final value $\alpha = 1$ (see the curve with $\alpha_0 = 1$). It is evident also that large acceleration values ($\dot{\alpha} > 1$) are observed only during a very short time interval at the end of the acceleration process. In a plot (see Fig. 46) of the path $S$ traveled by the beam front we can see a break which is typical for this moment, for pressures in the plateau region. In Fig. 47 we have shown the change with time of the charge neutralization. The charge neutralization changes like the velocity $\alpha$, i.e., at pressures in the plateau region there is a rapid rise of $\varkappa$.

The theory which has been developed gives a reasonable explanation of the behavior of the beam front, but it is not able to describe correctly the energy spectrum of the ions. The reason for this is that (as was discussed earlier) ions which are accelerated to the forward edge of the beam during its slow motion can be captured and accelerated again by the head part of the beam during its fast motion. In order to describe this mechanism of two-stage acceleration, we assumed that the beam front moves in accordance with the theory developed, and modeled the motion of the ions by means of a computer.[61,62] The ions were modeled as macroparticles with increasing weights which were determined by the ionization probability (72). The probability was assumed constant in the head part of the beam and equal to zero outside it. After the ions are produced, a constant force $F = ZeE/d$ acts on them inside the head part of the beam until they escape through its rear edge. For each value of $\alpha_0$ we used up to 5000 ions. In the numerical modeling we traced the space-time behavior of the ion density and energy and the change with time of the ion energy spectrum.

The time evolution of a typical spectrum is shown in Fig. 48. At $\tau = 1$ many ions are produced with low energy, and the front moves slowly. Most of the ions rush forward into the space in front of the beam, but they can penetrate only to a depth of the order $d_0$. At a moment of time $\tau = 2.0$ (shown in the figure) the front velocity is close to its final velocity, which is greater than the velocity of any ion. Ions which have escaped forward in this stage are captured and accelerated again, so that their energy eventually is eight times the initial energy of the electrons. We note that the group of fast ions is formed during the transient process just described. New fast ions no longer appear, since for $\alpha > 1$ the maximum ion energy is less than the electron energy.

The dependence of the maximum ion energy on the pressure $\alpha_0$ is given in Fig. 49. In the low-pressure region there is a slow rise of the ion energy. At a pressure above the critical value $\alpha_{0_{cr}} \approx 0.05$ a dependence close to quadratic is observed. Above a pressure value $\alpha_{co} \approx 1.5$ cutoff of the acceleration occurs (in contrast to the stationary case in which cutoff begins at $\alpha_{0_{co}} \approx 0.6$), and the rapid decrease of the ion energy indicates the upper limit of the pressure region in which acceleration is possible.

The numbers of ions whose energy is above one, two, or three electron energies are shown in Fig. 50 as a function of the pressure.

The number of ions has been normalized to the number of electrons in the head part of the beam divided by the charge state of the ion,

$$N_{i0} = \pi a^2 (2d_0)\, n_e/Z. \tag{86b}$$

We shall define the acceleration length as the path which is traveled by the head part of the beam until a stationary state is established. The model predicts an increase of the acceleration length with increase of the pressure, from $8d_0$ to $14d_0$ in the range of pres-

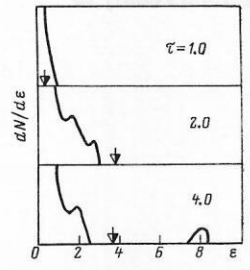


FIG. 48. Time evolution of typical energy spectrum of ions for $\alpha_0 = 1.4$. The arrows show the energy of an ion moving in the head part.

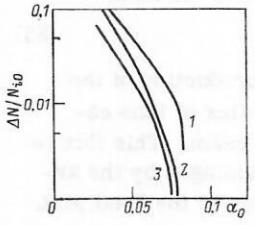


FIG. 50. Number of ions with energy exceeding a definite value (shown beside the curve) as a function of pressure. The normalization is explained in the text.

sures in which acceleration occurs.

*Scaling laws.* Knowing the structure of the model equations, we can derive simple laws which describe the dependence of the beam-front dynamics and ion acceleration on the experimental parameters. These parameters are the electron energy in the beam $W_0$, the beam current $I$ and its density $J$, the gas pressure $p$, the charge state $Z$, the mass and the ratio of the charge to the mass of the ion, and so forth.

The ionization probability $\nu_e$ depends on the cross section for ionization by electrons, and if the other experimental conditions are held constant it is proportional to the gas pressure $p$. Its dependence on the electron energy in the beam in the region of interest here is weak, and therefore we have

$$\nu_e \sim p. \tag{87}$$

The characteristic length is expressed only in terms of the beam parameters, namely in terms of the electron energy and the current density. From Eq. (15) we have

$$d_0 \sim \sqrt{W_0 \beta / J}. \tag{88}$$

The expression for the characteristic time contains the specific charge $Z/M$ of the ions. Use of Eq. (36) gives

$$\theta_0 \sim \sqrt{\frac{M}{Z}\frac{\beta}{J}}. \tag{89}$$

The dependence of $d_0$ and $\theta_0$ on the electron velocity can be neglected, since the value of the velocity $\beta$ at injection is close to unity. The model equations in dimensionless form contain only the parameters $\alpha_0$, $B$, and $\beta^*$.

Using Eqs. (87) and (88), we shall now write out the dependence of the dimensionless pressure defined by Eq. (75) on the parameters:

$$\alpha_0 \sim p \sqrt{\frac{M}{Z}\frac{\beta}{J}}. \tag{90}$$

The ratio of the cross sections for ionization by ions and by electrons $B$ for a given type of ion remains approximately constant.

The quantity $\beta^*$ is the normalized velocity of an ion with energy corresponding to the charge-exchange barrier. Since the velocity is expressed in units of $2\lambda_0/\theta_0$, we have

$$\beta^* \sim \sqrt{M/ZW_0}. \tag{91}$$

We shall scale the beam-front velocity in the plateau region by setting $\alpha \approx 1$, i.e.,

$$v_f \approx (2d_0/\theta_0) \sim \sqrt{ZW_0/M}. \tag{92}$$

We note that the velocity in the plateau region does not depend on the current. Let us consider the scaling in the ion charge state $Z$.

A complete discussion of the beam-front dynamics and acceleration of ions in gases with $Z > 1$ would be difficult, as the result of the need of introducing variables corresponding to ions of each charge state and the appearance of additional equations which take into account processes leading to change of the charge state of an ion (ionization, recombination). Therefore the theory developed here describes the case $Z = 1$ or an artificial situation in which an important role is played by ions with only one charge state $Z > 1$. Even in the last case $Z$-scaling in $\alpha_0$ and $\beta^*$ is difficult as a result of the fact that a change of $Z$ means a change of the type of atom and consequently a different behavior of the elementary processes.

However, for all quantities which do not depend on the elementary processes the dependence on $Z$ is correct (for a single charge state). The beam-front velocity (92) and the final energy of the ion are particularly important for the analysis. As was discussed in detail previously, the maximum velocity of an accelerated ion is $2v_f$ or $4v_f$, depending on whether the acceleration occurs in one or two steps. Therefore the ion energy $Mv^2/2$ is expressed in units of $Mv_f^2$ and, using Eq. (92) for the beam-front velocity, we have

$$W_i \sim ZW_0. \tag{93a}$$

Thus, the model predicts a linear dependence of the ion energy on its charge state and on the electron energy in the beam and no dependence on the ion mass.

One could attempt to replace $Z$ by an effective value taking into account the set of different charge states. However, as will be shown below, the situation is somewhat more complicated.

The case of a mixture of gases (different $Z/M$) has been discussed in detail by Alexander *et al.*[46] We shall consider first the situation in which ions of only one charge state $Z$ are present. The velocity in the plateau region, determined from Eq. (92), increases with increase of $Z/M$ and becomes greatest for hydrogen, when its maximum value is reached. If various ions are present in the head part of the beam, the front velocity in the plateau region is determined by the average behavior of the ions and will be less than the maximum possible value. In this case we will have selective acceleration of ions with the maximum ratio $Z/M$, while ions with a smaller value of $Z/M$ will move out of the head part of the beam. As a simple example which demonstrates the selective acceleration, in our model we have considered the case of a small admixture of $H_2(Z/M = 1)$ in $D_2$ $(Z/M = 1/2)$ in the drift tube. It was assumed that the motion of the beam front is determined by the deuterium, and the hydrogen ions are considered as test particles. We give the main results in this case below.

1. The velocity of $H^+$ ions is always greater than the velocity of $D^+$ ions.

2. In the plateau region the beam front moves with an average velocity determined by the two types of ions, and the influence of the light component turns out to be greater than would be expected on the basis of the gas concentration ratio in the mixture.

3. The intensity of the high-energy group of $H^+$ ions can be an order of magnitude greater than expected from the concentration ratio in the mixture. The calculation demonstrates the selective nature of the acceleration: acceleration of all kinds of ions except the

lightest component is suppressed. The explanation is that in the plateau region the beam front moves with a velocity which exceeds the critical value for $D^+$ ions but is subcritical for $H^+$ ions. The presence of hydrogen permits the beam to move more rapidly than in acceleration of deuterium alone. The electron beam attempts to move with the maximum possible velocity.

4. On increase of the concentration of $H_2$ in the mixture up to several percent, a comparison of the intensities of accelerated hydrogen and deuterium ions shows a rapid rise for high-energy protons. In this region the total intensity is even significantly greater (by more than a factor of two), than for filling with pure hydrogen. This is easily explained, since the beam-front velocity remains subcritical with respect to hydrogen and a larger number of $H^+$ ions are accelerated.

For a mixture of arbitrary gases with the presence of ions with $Z > 1$ we should expect results similar to those described above. The beam-front velocity will be determined as the average over velocities corresponding to the various components, the lightest components (maximum value of $Z/M$) entering with the greatest weight.

The lightest component is accelerated preferentially. Since in the drift chamber there is always an admixture of hydrogen, with filling by any gas we should see accelerated protons.

The scaling of the normalization of the number of accelerated ions (86b) is

$$N_{i0} \sim 1/Z. \tag{93b}$$

According to our previous remarks, Eq. (86b) determines the upper limit of the number of ions with $Z > 1$, since as a result of the presence of the lighter component the beam-front velocity becomes greater than the critical value for such ions.

We shall mention here only energy–current scaling, which leads to a decrease of the ion energy with increase of the current (current density) in accordance with the experimental data but contradicts the theory of Olson,[28,93] which predicts that in the high-pressure region the ion energy and the beam-front velocity will be independent of the current.

In addition let us point out the scaling of $p$ as a function of $J$ from Eq. (90). This can be seen distinctly by means of Figs. 23 and 26 by comparing the proton currents for different current densities. Kolomenskiĭ *et al.*,[20] and Drickey *et al.*[22] obtained maximum proton currents $J = 1$ kA/cm$^2$ and 5 kA/cm$^2$ at pressures $p = 0.1$ Torr and $p = 0.35$ Torr, respectively.

## Comparison with experiment

In this section we shall discuss the theory and compare the theoretical and experimental results. With some exceptions we shall follow the ideas developed in Sec. 2.

*Limiting current.* The most important feature of the experiments (see Table I) is the necessity that the current of the injected electron beam exceed the value of the electrostatic limiting current (11). Otherwise acceleration of ions is not observed. It is evident also from Table I that the Alfven–Lawson limiting current is not critical in experiments on ion acceleration (see above).

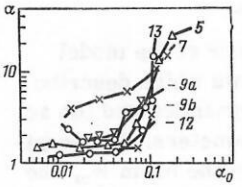


FIG. 51. Dimensionless beam-front velocity as a function of dimensionless pressure. The numbers denote the corresponding lines in Table I (see Figs. 3–5).

In a special series of experiments Straw and Miller varied the ratio $I/I_e$ over a wide range and confirmed that the condition $I/I_e > 1$ is necessary for acceleration of ions (see above). In addition the theory indicates a strong sensitivity of the ion acceleration process to $I/I_e$. In fact, the penetration depth of the electron beam (the basic scale of length in our theory) determined from Eq. (26) increases rapidly as $I/I_e - 1$, stopping of the beam is hindered, and creation of a strong electric field is difficult. The experiments of Straw and Miller confirm this conclusion: they observed an increase in the number of ions by three orders of magnitude on change of $I/I_e$ from 1.3 to 2.2 (see above).

*Beam-front dynamics.* The dependence of the stationary velocity of the beam front, predicted by the theory, on the dimensionless pressure is shown in Fig. 44. The experimental data (see Figs. 3–7) qualitatively manifest the same dependence on pressure, i.e., a more or less expressed plateau region at low pressures, and high velocities at a pressure exceeding some critical value. We reduce Figs. 3, 4, and 7 to a unified coordinate plane (Fig. 51) with use of the variables $\alpha$ and $\alpha_0$ instead of $\beta_f$ and $p$. This figure clearly confirms the scaling results applying to velocity and pressure. We shall discuss scaling in beam energy separately. From Eq. (92) we have $v_f \sim \sqrt{W_0}$, which is qualitatively confirmed by the data shown in Figs. 3 and 7.

In order to achieve quantitative agreement between theory and experiment we shall use for the probability of ionization by electrons the formula

$$\nu_e \approx 1.8p \ [\text{Torr} \cdot \text{nsec}]^{-1}, \tag{94}$$

which gives a value nine times higher than that given previously in Eq. (55). Equation (94) corresponds to an electron energy of only 100 eV (see Fig. 42), whereas Eq. (55) is valid in the range 0.3–4 MeV. In accordance with the idea of a virtual cathode we shall assume that in the head part of the beam there are many slow electrons. These electrons increase the average probability of ionization. Further, the experimental data indicate that in the plateau region $\alpha > 1$. In order to reconcile theory and experiment one can assume that the

beam potential is $\delta$ times greater than the electron energy, as was discussed in detail above. Then $d_0 \to d_0\sqrt{\delta}$ and, since $\alpha \sim v_f/d_0$, the value of $\alpha$ corresponding to fixed $v_f$ is decreased by $\sqrt{\delta}$ times. Agreement of experiment and theory is obtained with $\delta = 2$. It is evident from Fig. 51 that at high pressures the velocity reaches significantly higher values than the theory predicts.

A similar difficulty, possibly, appears in discussion of the data of Kolomenskiĭ *et al.* (Fig. 5) and Tkach *et al.* (Fig. 6). Let us first consider Fig. 5 and the data on hydrogen and helium in Fig. 6. On the one hand, in the plateau region scaling of the beam-front velocity gives $v_f \sim \sqrt{Z/M}$ [see Eq. (92)]. Therefore the maximum velocities should be achieved by hydrogen, which is confirmed by the data. On the other hand, at high velocities the theory predicts that the beam-front velocity will depend on the type of residual gas only through the rate of ionization by electron impact, so that for the two hydrogen isotopes (Fig. 5) we should expect equal velocities at high pressure. Similar arguments are valid for the data of Tkach *et al.*, which are still harder to explain as a result of the presence of multiply charged ions, as was discussed above.

We reach the conclusion that if we restrict the discussion to the low-pressure regime in the plateau region (which is important in ion acceleration), we can speak of reasonable agreement between theory and experiment for the dependence of the stationary velocity of the beam front on pressure.

Measurements of the path length traveled by the beam front as a function of time (Fig. 8) show that initially the beam moves very slowly, and then it abruptly acquires its final high velocity. Just such behavior is predicted by the theory (Figs. 45 and 46). The different values of the final velocity in Fig. 8 can be explained as follows. In the region beyond the plateau we have $\alpha \sim \alpha_0$, i.e.,

$$v_f \sim \frac{d_0}{\theta_0}\theta_0 = d_0 \sim \frac{1}{\sqrt{I}},$$

so that with increase of the current the beam-front velocity decreases in the vicinity of the plateau. The current in the beam for curve 1 is 43 kA, and for curves 2 and 3 it is about 80 kA. The same scaling ($\alpha \sim \alpha_0$) is expected for very low velocity values. We could consider that Fig. 8 confirms this prediction if the error in the measurements in this region were not so large.

Some understanding of the structure of the electric field can be achieved by using the data of Straw and Miller, which are shown in Fig. 10. It is important that the acceleration length, i.e., the distance from the anode at which accelerated ions are detected, decreases with increase of $I/I_e$, and the field at a high beam current is mainly axial, which agrees with the theory. The predicted value for the acceleration length lies in the range $(8-14)d_0$, which also is confirmed by the data of Table I and the results of Kolomenskiĭ *et al.*,[20] which are shown in Fig. 19. The appearance of radially accelerated ions can be explained by noting that the surface of the virtual cathode is mainly perpendicular to the beam axis and its geometry has a three-dimensional nature, in order to capture the head part of the beam. Since ion trajectories are primarily perpendicular to the surface of the virtual cathode, radially accelerated ions are observed. The virtual cathode does not move in the radial direction, and therefore the ion energy is equal in order of magnitude to the electron energy. In the experiments of Šunka *et al.*[25] various shapes of the virtual cathode were produced as the result of use of a plasma prepared beforehand. For a plasma with a sharp boundary, mainly axial ions appeared, while for a plasma with a smooth boundary there were more radial ions than axial ions.

The attempts of Bystritskiĭ *et al.*[26,27] to measure the potential directly in the drift space apparently refute the hypothesis of a deep potential well in Olson's theory,[28] but more accurate measurements are desirable.

*Energy of ions.* The stationary theory (41) predicts for a given beam-front velocity a maximum ion energy equal to $ZW_0(1+\alpha)^2$. Since $\alpha \sim v_f\sqrt{Z/M}$ from Eq. (35), it would appear that there is no simple scaling of the energy normalized to $W_0$ in $Z$, and that there is no dependence on the mass. It is important that in the plateau region where the ions are accelerated to the maximum energy there is scaling. Here $\alpha \approx 1$ and the energy is

$$W_i \sim ZW_0 \tag{95}$$

and does not depend on the mass. This scaling is clearly visible in the experimental data shown in Figs. 11 and 12. Similar arguments remain in force for the two-step acceleration mechanism.

The predicted pressure dependence of the energy is shown in Fig. 49 and is confirmed by the experimental data (Figs. 13–16). At low pressures corresponding to the beginning of the plateau region the energy is almost constant, then at the end of the plateau it increases, to achieve its maximum value (as the result of two-step acceleration) beyond the plateau region. At pressures $\alpha_0 > \alpha_{c0}$ ($\alpha_{c0}$ is the pressure corresponding to cutoff of acceleration) the ion energy decreases rapidly (see Fig. 16).

As was discussed above, the dependence of the ion energy on the current and on the current density have been studied in careful experiments. The theory predicts decrease of the ion energy with increase of the current density. Actually from Fig. 49 we have $\partial\varepsilon/\partial\alpha_0 > 0$ in the acceleration region. Since $\alpha_0 \sim \theta_0$ and $\theta_0 \sim 1/\sqrt{J}$ according to Eq. (89), we have $\partial\varepsilon/\partial J < 0$.

It was shown above that all observations, including those which contain obvious inconsistencies in the dependence on the current $I$, lead to this scaling.

*Characteristics of the ion pulse.* The number of accelerated ions as a function of the gas pressure, measured by several authors, is shown in Figs. 21–26. All data indicate existence of an optimal pressure at which the acceleration process is most efficient. The theoretical value of the accelerated-ion current density,

i.e., the density of ions which leave the beam through the forward edge of the head part, is shown in Fig. 44 as a function of $\alpha_0$ ($\sim p$). One can clearly see a maximum and a rapid drop of the intensity at high pressures. We note that $J_+$ has been normalized to the ionization probability $\nu_e$ in accordance with (71), so that at low pressures the current density decreases as the pressure drops. The latter is due to the lack of atoms which can be ionized. The theory predicts a linear decrease ($J_+ \approx 1$), in reasonable agreement with the experimental data.

The optimal pressure is determined from the condition of the maximum of the quantity $\alpha_0 J_+$, which is achieved near the lower limit of the plateau region.

According to Eq. (90) scaling of the optimal pressure should take the form $p \sim \sqrt{J/M}$. Scaling with respect to the current density is visible in Figs. 21 and 22. The dependence on the mass has no clearly expressed nature for small changes in mass (in Figs. 21 and 23 the maximum for deuterium occurs at higher pressures than for hydrogen, while in Fig. 24 the reverse situation is observed), but is confirmed by the data on nitrogen (Fig. 25). In this case the theory predicts the correct value $p_{opt} = (1/\sqrt{14})\, p_{opt}(H_2) \approx 0.027$ Torr, where $p_{opt}(H_2) \approx 0.1$ Torr has been taken from other data.

The scaling of $J_+$ contains the number of electrons $N_e$ in the head part of the beam [see Eqs. (71) and (66)] and $N_e \sim n_e d_0 \sim \sqrt{J}$, and therefore we should expect an increase of the ion intensity with increase of the current density. Figures 21 and 22 are consistent with this statement, but in this case the increase of intensity is mainly due to enhancement of the inequality $I/I_e > 1$, which is important for the acceleration process.

It apparently follows from Fig. 26 that the proton flux is greater for lower current densities (the total fluxes in the two cases are identical). Drickey *et al.*[22] pointed out that their data varied greatly from shot to shot (by more than an order of magnitude) for a constant $H_2$ pressure. Therefore we shall neglect this lack of correspondence of theory and experiment in the question of scaling of the ion intensity with the current density.

A further difficulty is related to the second maximum in Fig. 23 for hydrogen. It appears as the result of aperture effects due to instability of the radial motion of the ion beam at high pressures. The second maximum is not observed in studies by other authors.

A series of typical time dependences of the ion current pulse measured at 50 cm from the anode are shown in Fig. 29. The theory predicts that the pulse width $\tau$ should change in proportion to $\theta_0$, i.e., $\tau \sim \sqrt{M/Z}$, which is in reasonable agreement with the experimental data. The total number of ions should be inversely proportional to $Z$ [see Eq. (93)]. This dependence is confirmed if we exclude the data on nitrogen, with integration of the current pulse over time.

We estimate the number of ions in order of magnitude by means of Eq. (86b) to be $N_i = 2d_0 \pi a^2 n_e / Z$. From Table I (line 19) we find $d_0 = 1.2$ cm and $I = 30$ kA. Since $\pi a^2 n_e = \pi a^2 J_e / ev = I/ev$, for $Z = 1$ we obtain approximately $10^{13}$ ions. The signal for hydrogen integrated over time gives (200 A)$\cdot$(5 nsec/$e$). The agreement between theory and experiment is satisfactory.

The existence of several ion pulses, which is well confirmed experimentally, is predicted by the theory and has already been discussed in detail. In certain pressure regions the appearance of two pulses of high-energy ions may be the consequence of a two-step acceleration mechanism (see Figs. 40 and 41). In addition the theory predicts the appearance of a large group of slowly moving ions, those which left the head part of the beam in the early stage. They were observed by Ecker,[43] who studied the behavior of the ion current pulse over an extended time interval. The difference in time between the appearance of the fast and slow groups amounts to 70 nsec (for protons with energy 1 MeV and a flight path 1 m) and is in reasonable agreement with Ecker's data (100 nsec). The increase in the repetition frequency of pulses observed by Rander *et al.*[18] with increase of the pressure is difficult to compare with theory, since by means of Fig. 40 one cannot determine what occurs as a result of the change of pressure. The existence of multiple pulses was the starting point in a recently suggested theory of ion acceleration based on the appearance of the so-called focusing instability of an essentially force-free electron beam.[94] We note that the electrostatic model described for acceleration at the ionization front completely explains the appearance of several pulses.

The measured energy and momentum spectra of the ions are shown in Figs. 30–33. Most of the spectra have only one maximum, which is located between $W_0$ and 3 $W_0$ ($W_0$ is the electron energy). The data of Straw and Miller (Fig. 31) indicate appearance in the spectrum of a distinctly expressed group of ions with high energy (about $6W_0$) at the highest value of $v/\gamma$. The structure of this spectrum agrees qualitatively with the theoretical prediction for the maximum achievable ion energy. Very slow ions (with energy much less than $W_0$) usually are not observed. This is apparently due to the effect on the ions of the magnetic field of the beam in the region of almost complete charge neutralization.

Neglecting the disagreement on the question of slow ions, it can be stated that the two-step acceleration mechanism, which leads to a wide range of possible final spectra (see Fig. 41), is capable of explaining the experimental results. We shall establish a correspondence between the experimental data and the regions in Figs. 40 and 41. The spectrum in Fig. 32 is region I, the spectrum in Fig. 37 is region VI, and all of the remaining spectra are regions II, III, or IV.

The assumption of existence at the beam front of a potential well open on one side (a potential drop) is basic in our model. From this it necessarily follows that ions can have a velocity greater than the beam-front velocity (up to $4v_f$ under favorable circumstances) and can escape forward beyond the front. A direct proof can be obtained by using the results of study of the correlation of the velocities of the front and the ion beam,[22] which are shown in Fig. 34: the protons move

faster than their beam front in most cases, confirming our assumption and refuting the hypothesis of synchronous motion of the beam front and the ion bunch, which corresponds to a potential well closed on both sides.

In the question of synchronous motion we disagree substantially with Olson,[28] who attempts to explain the equal velocities of the ion and beam front by means of the following assumption: the fastest ions are produced in the initial phase (suppression of the beam), extending the equilibrium potential well in such a way that the front propagates consistently with the velocity of the fast ions. This proposed *ad hoc* mechanism is unlikely because the positive ions would raise the potential at the forward edge of the well and thus would shorten it.[46]

In other experiments, described above, the ion velocities were either equal to the front velocity (Ref. 17; Tables II and III of the present article) or much less than the front velocity.[20,29] In regard to the experiments of Graybill, comparison of the data was carried out with use of front velocities in the high-pressure regime. In the region typical of ion acceleration the front velocities are significantly lower (see Ref. 22 in Ref. 64).

We mentioned previously that the front velocities measured by Kolomenskiĭ *et al.*[20] are not explained very well from the point of view of scaling in mass at high pressures. We add here that even in the plateau region the velocities are higher than the expected values.

We note that in the general case slow ions can appear when the beam front has velocity $\alpha \gg 1$, which leads to cutoff of acceleration (the ions escape from the head part backward). This statement is valid for a closed potential well and for a potential well open on one side. Motion of ions with velocity greater than the front velocity, on the other hand, cannot be explained with use of a closed potential well.

A possible mechanism which can lead to a high front velocity is preliminary ionization by electrons and ions (see above). This effect was not accurately taken into account in the theory described here, but earlier calculations showed that in this case the front velocity increases somewhat.[39] From comparison of the velocities we conclude that in accordance with our theory the recorded ions move more rapidly than the beam front. The presence of slow ions is consistent with the theory.

According to the ideas which have been developed, the bunch of fast ions should be located in front of the head part. In experiments the ion bunch has been recorded in the head part (in most cases), immediately behind it,[22] or far from it (Ref. 19; Fig. 35 of the present article).

This obvious contradiction can be removed if we consider carefully the concept of beam front. On the one hand the beam front is identified from the rapid rise of current in the Rogowski belt. In the theory the beam front is determined by the location of the virtual cathode, which approximately coincides with the place where the beam current is equal to the limiting current.

Assuming the rise of the current to be linear, we find for the distance between the current front and the virtual cathode[12)]

$$\Delta x \geqslant v_f t_r I_e / I_{\max}. \tag{96}$$

In this inequality we have taken into account the possibility of partial neutralization of the space charge [see Eq. (28)], as a consequence of which the true value of the limiting current is greater than the limiting value in vacuum (11). For the experiments of Drickey *et al.*[22] from line 9 of Table I we find $t_r \approx 10$ nsec, $I = 100$ kA, $I_e = 7.1$ kA and from Fig. 27 $v_f \approx (0.07-0.17)c$, which gives $\Delta x \approx 1.5-3.6$ cm. Ecker *et al.*[19] (line 13 of Table I) used a current pulse with a rate of rise $7.5 \times 10^{12}$ A/sec during the first 10 nsec, so that the limiting current $I_e = 10.3$ kA was achieved after 1.4 nsec. From Fig. 35 we have for hydrogen $v_f \approx 0.15c$, so that $\Delta x \approx 6.3$ cm. This distance is 2–3 times larger than Drickey's value and we can speak at least of qualitative agreement with the observations.

It must be emphasized again that we have calculated only the lower limit for the distance between the current front and the virtual-cathode location. The actual value may be (and actually is) significantly larger.

Regarding the data of Graybill *et al.*[29,30] we recall the remark made earlier in this section on comparison of the velocities. The data on nitrogen in Fig. 35 show that at the beginning of the acceleration process the value of $\Delta x$ is the same as for hydrogen, but with time it rises linearly. This is explained by the escape of ions from the head part of the beam backward as the result of the high velocity of the front, i.e., for nitrogen we already have $\alpha > 1$, whereas for hydrogen $v_f$ can still remain such that $\alpha$ is in the plateau region ($\alpha \approx 1$).

We have reached the concluding question of this section: selective acceleration of ions with the maximum charge-to-mass ratio. As was indicated, our model predicts in a natural way the predominant acceleration of the lightest components in a gas mixture. It has found confirmation in many experiments, being a side result, since in all vacuum systems used, hydrogen is always present. A special series of careful experiments carried out by Kolomenskiĭ *et al.*[47] (Table V) gave good agreement with theory.

*Other dependences.* We shall now discuss the influence of a longitudinal magnetic field $B$, of pressure gradients, and of changes in the beam-front rise time.

The theory predicts the existence of two main effects which arise on application of a magnetic field:

1) part of the limiting current $I_e$ should propagate over the entire length of the system, since scattering of the beam is suppressed;

2) the mobility of the secondary electrons decreases

[12)] Rander[17] observed that the shape of the electron current pulse does not change substantially on drift of the beam. This justifies the use of $v_f$ in Eq. (96).

under the action of a magnetic field, and they move along the drift tube mainly in the longitudinal direction.

Of these two effects, the latter leads to an increase of the effective time of charge neutralization in the drift region (as was observe by Bystritskiĭ *et al.*[26]), while the former leads to a very important consequence: over the entire drift region, and not in a small part of it near the entrance plane in the case $B=0$, neutralization of the space charge sets in. Spatially uniform neutralization leads to a rapid change of the potential well. In addition, there is no moving virtual cathode. It is clear that this situation differs greatly from that discussed previously and acceleration of ions should not be expected.

A critical external magnetic field should compensate the self-field of the beam, under the action of which the beam tends to expand in the radial direction. For $B_{cr}$ we obtain an estimate

$$B_{cr} \approx \frac{\mu_0 I}{2\pi a} \frac{1}{\gamma_{av}^2 - 1}, \tag{97}$$

where $\gamma_{av}$ is the average value of the factor $\gamma$ in the longitudinal and azimuthal directions.

The current of the transmitted beam is

$$I_{trans} \approx I_e \min(1,\ B/B_{cr}). \tag{98a}$$

From the data of Ecker *et al.*[19] (line 13 of Table I), using $\gamma_{av} \approx 3$, we have $B_{cr} \approx 0.2$ kG, which is in good agreement with the absence of ions for $B=0.2$ kG in their experiment.

The influence of the rise time of the front on the acceleration process can be understood in the following way. A necessary condition for creation of a virtual cathode is an excess of the beam current over the limiting current value. Taking into account that the limiting current depends on time through the degree of charge neutralization and the energy of the electron, we write this condition in the form

$$I(t) = I_{max} \frac{t}{t_{rI}} \geqslant I_e \max(1,\ t/t_{rv})/(1 - v_{ef}t), \tag{98b}$$

where $t_{rI}$ and $t_{rv}$ are the rise times of the current and voltage and $I_e$ is the limiting current in vacuum (11) for $t_{rv}=0$. Considering the two cases individually for $\max(1, t/t_{rv})$, we arrive at the following inequality:

$$t_{rI} \leqslant \frac{I_{max}}{I_e} \min\left(t_{rv},\ \frac{1}{4} t_{ef}\right), \tag{99}$$

where $t_{ef} = 1/\nu_{ef}$. For equal rise times we have

$$t_r < \frac{I_{max}}{4I_e} t_{ef} \tag{100}$$

and since $t_{ef} \sim 1/p$ we arrive at the condition that the product of the rise time by the pressure does not depend on the latter: $t_r p = \text{const}$. This condition is in agreement with the results of Kolomenskiĭ *et al.*[45]:

1) for two different rise times ($t_r = 10$ nsec and 30 nsec; see Fig. 37) the optimal pressure, at which the ion energy is maximal, satisfies the condition $p_{opt} t_r = 5$–$6$ Torr · nsec;

2) the ion energy is the same in the two cases.

The latter result is to be expected, since when the condition for the rise time is satisfied a virtual cathode is formed and the acceleration process begins.

The effect of positive and negative pressure gradients has been studied in several papers with the aim of controlling the motion of the beam front and increasing the efficiency of the acceleration process. We shall consider briefly the promise of this idea, resting mainly on the experimental data.

At least three problems must be solved: 1) control of the beam-front velocity; 2) capture of ions in its head part; 3) acceleration of the beam front without loss of ions.

In discussion of the first point the following question arises: do the values of the front velocity with variation of the pressure along the length agree with the values calculated in the stationary model? Our theory predicts that this is valid for an adiabatic pressure value, where we have an acceleration $\dot{\alpha} < 1$. The theory of Olson,[95,28] on the other hand, states that only the length of the head part of the beam changes, while the front velocity remains constant. The experiments of Tkach[21] convincingly confirm the change of the front velocity.

It must be pointed out that both in theory and experiment the transition of the front velocity from very small values ($\alpha \approx \alpha_0$) to large values $\alpha \approx 1$ has a nonadiabatic nature ($\dot{\alpha} > 1$). It is just this stage which determines both the number of ions captured and their velocities. On the other hand, this discontinuity cannot be controlled, since it is an inherent property of the gas–beam–ion system.

During this phase it is possible to obtain capture of a certain group of ions. For capture it is necessary, first, that the ions not be behind the beam front, and second, that the front velocity not exceed the ion velocity by more than $\alpha = 1$. As was discussed previously, frequently these conditions are not satisfied in experiments.

We shall assume that capture of a group of ions has occurred and that they are moving with an experimentally determined velocity in the plateau region. Choosing the maximum value of acceleration at which capture still exists ($\dot{\alpha} = 1$), we find for the acceleration lengths in certain typical experiments the following values: $l = 8.7$ cm (line 5 of Table I), $l = 18.2$ cm (line 13 of Table I), and $l = 54$ cm (line 7 of Table I). We note that Kolomenskiĭ *et al.* obtained shorter acceleration lengths, but only for ions having velocities a factor of two less than the corresponding front velocities (at the same pressures). Let us now determine the pressure gradients necessary for further acceleration of the captured ions (with use of the experimental dependence of velocity on pressure). Assuming that the acceleration $\dot{\alpha}$ is constant and satisfies the condition $\dot{\alpha} < 1$, so that the fraction of ions not captured into the acceleration process, which is approximately equal to $\dot{\alpha}$, is small, we find the following pressure changes ($\dot{\alpha} = 0.1$): Rander *et al.*, $p = 0.5$–$1.0$ Torr in 42 m, $p = 0.6$–$0.8$ Torr in 22.5 m, and Kolomenskiĭ *et al.*, $p = 0.2$–$0.5$ Torr in 34 m. It follows from this that very small

pressure gradients are necessary. The smallest of the pressure gradients used in Ref. 52 (Fig. 9) was 0.1 Torr/m, which corresponds to $\dot{\alpha} \approx 1$. In this case, consequently, there should be no positive effects, which agrees with the experimental results of Kuswa.

In the preceding discussion we arrive at the conclusion that achievement of a positive effect in ion acceleration with use of a pressure gradient is difficult, since it is impossible to control the capture of ions (problem 2) and for their subsequent acceleration it is necessary to create conditions on the pressure gradient which are difficult to realize (problem 3).

The acceleration process has been studied with a step change of the pressure experimentally by Kolomenskiĭ *et al.*[47] and studied numerically in the one-dimensional model by Hintze *et al.*[62] The results of the theoretical investigation indicate the possibility of some increase of ion energy and a significant increase of the number of ions. The disagreement with experiment is explained by the too short length of the second portion of the drift space in the experiment.

## CONCLUSION

The present work has pursued two goals. First, we have given a comprehensive review of experimental results on collective uncontrolled acceleration of ions in propagation of a high-current electron beam in a low-pressure gas. Second, we have examined in detail the model of acceleration in the ionization front. Comparison of theory and experiment shows that to a first approximation it is possible by means of a one-dimensional electrostatic mechanism to explain all of the experimental data. The main emphasis has been on the qualitative agreement obtained with use of the scaling laws introduced in the model.

Many authors have attempted to use the knowledge in this field, accumulated in many years of theoretical and experimental studies, for the purpose of going over from the process of acceleration under natural conditions to controlled acceleration schemes.[93] The most promising of these is the IFA (ionization-front accelerator) proposed by Olson in 1973.[66,96,7] In this scheme a beam is injected into a working gas at a very low pressure, such that the beam cannot propagate and a potential well is formed. Then the working gas is ionized by a laser beam which is scanned along the drift tube according to a specified program, so that the potential well with the captured ions moves according to a previously determined law. Although Olson *et al.*[8] obtained the first experimental results which confirm the possibility of realization of the IFA, the viability of this ion-acceleration scheme still awaits verification.

The authors express their gratitude to A. A. Kolomenskiĭ, V. M. Likhachev, and K. Jungwirth for numerous helpful discussions.

[1]V. I. Veksler, Proc. CERN Symposium, 1956, Vol. 1, p. 80.
[2]V. I. Veksler, At. Énerg. 2, 427 (1957).
[3]M. S. Rabinovich, Preprint FIAN-36, Moscow, 1969; UCRL Translation 1398, Berkeley.
[4]M. S. Rabinovich and V. N. Tsytovich, Tr. Fiz. Inst. Akad. Nauk SSSR 66, 7 (1973).
[5]M. S. Rabinovich and V. N. Tsytovich, Preprint FIAN-55, Moscow, 1973.
[6]S. E. Graybill and J. R. Uglum, J. Appl. Phys. 41, 236 (1970).
[7]C. L. Olson, in: First Intern. Topical Conf. on E-Beam Research and Technology, Vol. 11, Albuquerque, New Mexico, USA, 1975, p. 312.
[8]C. L. Olson *et al.*, IEEE Trans. Nucl. Sci. 24, 1659 (1977).
[9]C. L. Olson, in: Third Intern. Conf. on Collective Methods of Acceleration, Laguna Beach, Calif., USA, 1979, p. 305.
[10]A. A. Plyutto, Zh. Eksp. Teor. Fiz. 39, 1589 (1960) [Sov. Phys. JETP 12, 1106 (1961)].
[11]A. A. Plyutto *et al.*, Pis'ma Zh. Eksp. Teor. Fiz. 6, 540 (1967) [JETP Lett. 6, 61 (1967)].
[12]J. S. Luce, H. L. Sahlin, and T. R. Crites, IEEE Trans. Nucl. Sci. 20, 336 (1973).
[13]J. S. Luce, Ann. N. Y. Acad. Sci. 251, 217 (1975).
[14]V. P. Smirnov, Prib. Tekh. Eksp., No. 2, 7 (1977) [Instrum. Exp. Tech. 20, 337 (1977)].
[15]R. F. Hoeberling and D. N. Payton, J. Appl. Phys. 48, 2079 (1977).
[16]F. C. Young and M. Friedman, J. Appl. Phys. 46, 2001 (1975).
[17]J. Rander, Phys. Rev. Lett. 25, 893 (1970).
[18]J. Rander *et al.*, in: Physics Intern. Company Project 50-147. Final Report, 1971.
[19]B. Ecker, S. Putnam, and D. Drickey, IEEE Trans. Nucl. Sci. 20, 301 (1973).
[20]A. A. Kolomenskiĭ *et al.*, Preprint FIAN-44, Moscow, 1975.
[21]Yu. V. Tkach *et al.*, Zh. Tekh. Fiz. 44, 658 (1974) [Sov. Phys. Tech. Phys. 19, 412 (1974)],
[22]D. Drickey, B. Ecker, and S. D. Putnam, in: Ninth Intern. Conf. on High Energy Accelerators, Stanford, Calif., 1974, p. 658.
[23]G. W. Kuswa, L. D. Bradley, and G. Yonas, IEEE Trans. Nucl. Sci. 20, 305 (1973).
[24]R. B. Miller and D. C. Straw, J. Appl. Phys. 47, 1897 (1976).
[25]P. Šunka *et al.*, in: Eighth European Conf. on Controlled Fusion Plasma Physics, Prague, Vol. 1, 1977, p. 108.
[26]V. M. Bystritsky *et al.*, in: Seventh Intern. Symposium on Discharges in Electrical Insulators in Vacuum, Novosibirsk, 1976, p. 362.
[27]V. M. Bystritskiĭ *et al.*, Pis'ma Zh. Tekh. Fiz. 2, 991 (1976) [Sov. Tech. Phys. Lett. 2, 389 (1976)].
[28]C. L. Olson, Phys. Fluids 18, 585 (1975).
[29]S. E. Graybill, IEEE Trans. Nucl. Sci. 18, 438 (1971).
[30]S. E. Graybill, IEEE Trans. Nucl. Sci. 19, 292 (1972).
[31]A. A. Kolomenskiĭ *et al.*, Zh. Eksp. Teor. Fiz. 68, 51 (1975) [Sov. Phys. JETP 41, 26 (1975)].
[32]B. Ecker and S. D. Putnam, IEEE Trans. Nucl. Sci. 24, 1665 (1977).
[33]B. Ecker and S. D. Putnam, in: Second Symposium on Collective Methods of Acceleration, Dubna, 1976, p. 152.
[34]D. C. Straw and R. B. Miller, J. Appl. Phys. 47, 4681 (1976).
[35]D. C. Straw and R. B. Miller, in: IEEE Intern. Conf. on Plasma Science, Austin, Texas, 1976, p. 130.
[36]D. C. Straw and R. B. Miller, Appl. Phys. Lett. 25, 379 (1974).
[37]K. F. Alexander, E. Hantzsche, and P. Siemroth, Preprint, Akad. Wiss. DDR, Berlin, 1973.
[38]K. F. Alexander, in: Festschrift wiss. Koll. 65 Geburtstag, R. Rompe, Akad.-Verlag, Berlin, 1973, p. 21.
[39]K. F. Alexander, E. Hantzsche, and P. Siemroth, Zh. Eksp. Teor. Fiz. 67, 567 (1974) [Sov. Phys. JETP 40, 280 (1974)].
[40]V. M. Bystritskiĭ *et al.*, Pis'ma Zh. Tekh. Fiz. 2, 80 (1976) [Sov. Phys. Tech. Phys. Lett. 2, 30 (1976)].
[41]R. B. Miller and D. C. Straw, in: Intern. Topical Conf. on Electron Beam Research and Technology, Albuquerque,

New Mexico, USA, 1975.
[42]A. A. Kolomenskiĭ and M. A. Novitskiĭ, Kratkie soobshcheniya po fizike (Brief Communications in Physics) **10**, 37 (1976).
[43]B. Ecker, Private communication, 1976.
[44]J. Rander *et al.*, Phys. Rev. Lett. **24**, 283 (1970).
[45]A. A. Kolomenskii *et al.*, in: Trudy VI Vsesoyuznogo soveshchaniya po uskoritelyam zaryazhennykh chastits (Proc. of the Sixth All-Union Conf. on Charged-Particle Accelerators), Vol. 2, Dubna, 1979, p. 31.
[46]K. F. Alexander and W. Hintze, in: Second Symposium on Collective Methods of Acceleration, Dubna, 1976, p. 155.
[47]A. A. Kolomenskii *et al.*, in: Second Symposium on Collective Methods of Acceleration, Dubna, 1976, p. 114.
[48]C. L. Olson, in: Second Symposium on Collective Methods of Acceleration, Dunba, 1976, p. 101.
[49]C. W. Roberson *et al.*, Phys. Rev. Lett. **36**, 1457 (1976).
[50]T. Tajima and F. Mako, Phys. Fluids **21**, 1459 (1978).
[51]D. W. Swain *et al.*, in: Ninth Intern. Conf. on High Energy Accelerators, Stanford, Calif., 1974, p. 268.
[52]G. W. Kuswa, Ann. N.Y. Acad. Sci. **251**, 514 (1975).
[53]C. L. Olson, Part. Accel. **6**, 107 (1975).
[54]C. L. Olson, Ann. N. Y. Acad. Sci. **251**, 536 (1975).
[55]S. D. Putnam, Bull. Amer. Phys. Soc. **14**, 1048 (1969).
[56]S. D. Putnam, Phys. Rev. Lett. **25**, 1129 (1970).
[57]S. D. Putnam, IEEE Trans. Nucl. Sci. **18**, 496 (1971).
[58]N. Rostoker, Bull. Amer. Phys. Soc. **14**, 1047 (1969).
[59]N. Rostoker, in: Seventh Intern. Conf. on High Energy Accelerators, Erevan, 1969, p. 509.
[60]S. E. Rosinskiĭ, A. A. Rukhadze, and V. G. Rukhlin, Pis'ma Zh. Eksp. Teor. Fiz. **14**, 53 (1971) [JETP Lett. **14**, 34 (1971)].
[61]K. F. Alexander and W. Hintze, Preprint, Zentralinst. Elektronenphysik. Akad. Wiss. DDR, 76-7, Berlin, 1976.
[62]W. Hintze and K. F. Alexander, in: Thirteenth Intern. Conf. on Phenomena in Ionized Gases, Berlin, GDR, 1977, p. 11.
[63]C. L. Olson, Bull. Amer. Phys. Soc. **18**, 1356 (1973).
[64]C. L. Olson, Phys. Fluids **18**, 598 (1975).
[65]R. Davidson, Theory of Nonneutral Plasma, Banjamin, 1974. (Russ. transl., Mir, Moscow, 1978).
[66]C. L. Olson, Bull. Amer. Phys. Soc. **18**, 1369 (1973).
[67]C. L. Olson and J. W. Poukey, Phys. Rev. A **9**, 2631 (1974).
[68]B. B. Godfrey, IEEE Trans. Plasma Sci. **6**, 256 (1978).
B. B. Godfrey *et al.*, in: IEEE Intern. Conf. on Plasma Science, Troy, N.Y., USA, 1977, p. 174.
[69]G. I. Budker, in: CERN Symposium on High Energy Accelerators and Pion Physics, Vol. 1, Geneva, 1956, p. 68.
[70]C. L. Olson, Fiz. Plazmy **3**, 465 (1977) [Sov. J. Plasma Phys. **3**, 259 (1977)].
[71]L. S. Bogdankevich and A. A. Rukhadze, Usp. Fiz. Nauk **103**, 609 (1971) [Sov. Phys. Usp. **14**, 163 (1971)].
[72]C. K. Birdsall and W. B. Bridges, J. Appl. Phys. **32**, 2611 (1961).
[73]A. V. Pashchenko and B. N. Rutkevich, Fiz. Plazmy **3**, 774 (1977) [Sov. J. Plasma Phys. **3**, 437 (1977)].
[74]V. A. Godyak, L. B. Dubovoi, and G. R. Zabolotskaya, Zh. Eksp. Teor. Fiz. **57**, 1795 (1969) [Sov. Phys. JETP **30**, 971 (1970)].
[75]V. S. Voronin, Yu. T. Zozulya, and A. N. Lebedev, Zh. Tekh. Fiz. **42**, 546 (1972) [Sov. Phys. Tech. Phys. **17**, 432 (1972)].
[76]J. W. Poukey and N. Rostoker, Plasma Phys. **13**, 897 (1971).
[77]R. B. Miller and D. C. Straw, J. Appl. Phys. **48**, 1061 (1977).
[78]K. Jungwirth, in: Tenth Czech. Seminar on Plasma Physics Technology, Zvicov, 1979, p. 44.
[79]D. A. Phelps, IEEE Trans. Plasma Sci. **6**, 76 (1978).
[80]D. D. Ryutov and G. V. Stupakov, Fiz. Plazmy **2**, 767 (1976) [Sov. J. Plasma Phys. **2**, 427 (1976)].
[81]D. D. Ryutov, Zh. Tekh. Fiz. **47**, 709 (1977) [Sov. Phys. Tech. Phys. **22**, 709 (1977)].
[82]R. J. Lomax, J. Electron. Control **9**, 127 (1960).
[83]E. Hantzsche, Beitr. Plasmaphys. **15**, 157 (1975).
[84]E. Hantzsche, Beitr. Plasmaphys. **17**, 253 (1977).
[85]A. A. Kolomenskiĭ and M. A. Novitskii, Zh. Tekh. Fiz. **46**, 44 (1976) [Sov. Phys. Tech. Phys. **21**, 23 (1976)].
[86]J. W. Poukey and C. L. Olson, Phys. Rev. A **11**, 691 (1975).
[87]S. L. Ginzburg *et al.*, Preprint, Institute of Applied Mathematics, USSR Academy of Sciences, Moscow, 1980.
[88]P. M. Morse and H. Feshbach, Methods of Theoretical Physics, McGraw-Hill, N.Y., 1953 (Russ. transl., IIL, Moscow 1960).
[89]H. Alfven, Phys. Rev. **55**, 425 (1939).
[90]W. Hintze, Preprint, ZIE, 78-9, Berlin, 1978.
[91]W. Hintze, in: Third Intern. Topical Conf. on High Power Electron and Ion Beam Research and Technology, Vol. 1, Novosibirsk, 1979, p. 549.
[92]C. L. Olson, Phys. Rev. A **11**, 288 (1975).
[93]C. L. Olson, Collective Ion Acceleration with Linear Electron Beams, in: Springer Tracts in Modern Physics, Springer-Verlag, Berlin–Heidelberg–New York, 1979.
[94]K. V. Khodataev and V. N. Tsytovich, Fiz. Plazmy **2**, 301 (1976) [Sov. J. Plasma Phys. **2**, 164 (1976)].
[95]C. L. Olson, Bull. Amer. Phys. Soc. **19**, 914 (1974).
[96]C. L. Olson, in: Ninth Intern. Conf. on High Energy Accelerators, Stanford, Calif., 1974, p. 272.
[97]E. W. McDainel, Collision Phenomena in Ionized Gases, Wiley, N.Y., 1964. (Russ. transl., Mir, Moscow, 1967).
[98]R. A. Langley *et al.*, Phys. Rev. **136**, A379 (1964).
[99]F. F. Rieke and W. Prepejchal, Phys. Rev. A **6**, 1507 (1972).

Translated by Clark S. Robinson